

Article

Enhancing Signal-to-Noise Ratio in Vehicle-to-Vehicle Visible Light Communication Systems Through Diverse LED Array Transmitter Geometries

Ahmet Deniz , Melike Oztopal and Heba Yuksel * 

Department of Electrical and Electronics Engineering, Bogazici University, Bebek 34342, Istanbul, Turkey; ahmet.deniz@std.bogazici.edu.tr (A.D.); melike.oztopal.2024@alumni.boun.edu.tr (M.O.)

* Correspondence: heba.yuksel@bogazici.edu.tr

Abstract: In this paper, a novel method is introduced to enhance the performance of vehicle-to-vehicle (V2V) visible light communication (VLC) by employing different transmitter (Tx) light-emitting diode (LED) array arrangements with different LED orientations. Improving the signal-to-noise ratio (SNR) is crucial for V2V VLC systems to provide long communication ranges. For this purpose, six transmitter configurations are proposed: single-LED transmitters, as well as 3×3 square-, single hexagonal-, octagonal-, 5×5 square-, and honeycomb hexagonal-shaped LED arrays. Indoor VLC studies using LED arrays offer a uniform SNR, while outdoor studies focus on optimizing the receiver side to enhance system performance. This paper optimizes system performance by increasing the SNR and communication range of V2V VLC systems by changing the geometry of the Tx LED array and LED orientations. A V2V VLC system using on-off keying (OOK) is modeled in MATLAB, and the SNR and bit error rate (BER) are simulated for different Tx configurations. Our results show that the honeycomb hexagonal transmitter design provides a 19% improvement in system performance with a spacing of 1 cm, and maintains a 16% improvement when the array size is reduced by a factor of 100, making it smaller than one of the smallest industrial headlight modules.

Keywords: vehicle-to-vehicle communication; visible light communication; signal-to-noise ratio; bit error rate; maximum communication range; light-emitting diode arrays; field of view



Citation: Deniz, A.; Oztopal, M.; Yuksel, H. Enhancing Signal-to-Noise Ratio in Vehicle-to-Vehicle Visible Light Communication Systems Through Diverse LED Array Transmitter Geometries. *J. Sens. Actuator Netw.* **2024**, *13*, 69. <https://doi.org/10.3390/jsan13060069>

Academic Editor: Lei Shu

Received: 16 September 2024

Revised: 6 October 2024

Accepted: 8 October 2024

Published: 23 October 2024



Copyright: © 2024 by the authors. Licensee MDPI, Basel, Switzerland. This article is an open access article distributed under the terms and conditions of the Creative Commons Attribution (CC BY) license (<https://creativecommons.org/licenses/by/4.0/>).

1. Introduction

In recent years, visible light communication (VLC) has attracted remarkable attention due to the increasing demand for wireless communication technologies [1]. VLC provides countless advantages such as a license-free spectrum, low power consumption, high security, large spectrum capacity, high data rates, immunity to electromagnetic interference, and low latency [2–8]. Additionally, VLC offers improved spatial reuse, which is beneficial in densely populated areas [9,10]. Furthermore, VLC is less harmful than other wireless communication technologies for human health, provided the illumination level is below the eye safety level [11,12]. VLC can also be integrated into existing lighting infrastructure, making it a cost-effective solution for smart lighting and communication systems [13,14]. VLC systems can provide precise indoor positioning and navigation services, which are advantageous in various applications, including retail and healthcare [15,16]. Moreover, VLC supports high-speed data transmission and is considered an eco-friendly technology due to its energy efficiency [17,18].

In its simplest form, a VLC system typically consists of light-emitting diodes (LEDs) that transmit modulated light, and a photodetector functioning as a receiver to extract the data signal from the transmitted light beam. Using VLC technology in vehicle-to-vehicle (V2V) communication has the potential to prevent traffic accidents and provide efficient traffic management [19–21]. V2V VLC systems can also enhance the reliability of communication in environments where RF signals are prone to interference, such as

urban canyons and tunnels [7,22]. Moreover, V2V VLC offers the potential for high data rate transmission and low latency, which are crucial for real-time applications in intelligent transportation systems (ITS) [8,23,24].

Technological advancements in V2V VLC are drawing significant attention within the automotive industry. Numerous studies in the literature [25–27] have explored the application of VLC utilizing photodetectors instead of camera systems for automotive purposes. These studies highlight the potential of leveraging existing lighting infrastructure for communication. Additionally, this technology allows automotive companies to integrate V2V communication with minimal alterations into existing vehicle designs, primarily through minor modifications to current lighting systems [28,29]. The deployment of LEDs in vehicle headlights and taillights for communication purposes is particularly promising, as it represents a potential technology to enhance vehicle safety. However, increasing the signal-to-noise ratio (SNR) to provide a long communication range in a V2V VLC system is a challenge. To solve this problem, many studies have been conducted in the literature, with most studies focusing on improving V2V VLC systems by optimizing the receiver (Rx) side.

In [30], the misalignment effect in V2V VLC systems is evaluated with an experimental demonstration of a 75 m link. This paper also confirms that the optical filters and narrow field of view (FOV) obtained with optical lenses can significantly optimize a VLC receiver. In [31], a novel concept that uses LED current overdriving is introduced to increase the instantaneous optical irradiance and, in turn, the communication range.

In [32], it is discussed that the high mobility of vehicles necessitates an adaptive physical layer (PHY) design for reliable and rate-optimal communication. This paper proposes a novel low-complexity, location-aware adaptive PHY design that attains reliable, rate-optimal vehicular VLC without a feedback channel.

In [33], the achievable transmission distance for a targeted data rate while satisfying a bit error rate (BER) value is determined for different weather conditions. This study presents numerical results for clear, rainy, and foggy weather conditions and quantifies degradation from adverse weather conditions.

In [34], an analytical daylight noise model based on a modified Blackbody radiation model is proposed to capture the effect of ambient light noise and conduct an in-depth study on the impact of daylight on system performance. This study also proposes a selective combining receiver to improve the BER at the expense of a slight increase in the cost and complexity of the receiver.

In [35], the replacement of the traditional photodiode receiver with an imaging receiver is analyzed, showing that this replacement leads to improved performance with an increased SNR. In [36], an indoor cellular VLC system is proposed with hexagonal LED arrays to enhance the BER.

In [37], an indoor VLC system is analyzed. The system has sixteen LEDs on the ceiling that are used as transmitters. The paper aims to improve SNR uniformity throughout the room without increasing the number of transmitters on the ceiling. Instead, it considers altering the lamp arrangement and evaluates the uniformity of light and SNR distribution throughout the room.

In this paper, a V2V VLC system using on-off keying (OOK) is modeled in MATLAB, and the SNR and BER are simulated for different Tx configurations. The Pulse Position Modulation (PPM) and Non-Return-to-Zero (NRZ) modulation techniques are complex modulation methods preferred in certain applications [38,39]. PPM is used especially in applications requiring energy efficiency and low noise sensitivity, while NRZ offers the advantage of low cost in data transmission. However, the reason we preferred OOK modulation in this study is the simplicity, applicability, and widespread use of this modulation method in LED-based communication systems. OOK modulation offers the advantages of low complexity and easy implementation, making it ideal for performing a basic performance analysis of different geometric LED arrays. Therefore, PPM and NRZ modulations were not needed in our study.

Unlike most V2V VLC studies that are focused on the receiver side, by proposing six different transmitter LED array configurations to increase the SNR, this paper aims to optimize the transmitter side to improve the SNR of a V2V VLC system using OOK. The use of various arrangements of LED arrays is considered in the literature for indoor VLC to achieve light and SNR uniformity. However, this paper evaluates the enhancement in the SNR and, hence, the communication range that LED array transmitters of various geometries can achieve. In addition, we adjust the orientations of the LEDs to ensure that every configuration illuminates approximately the same area. This approach allows us to exploit the smaller FOV of each LED in the array transmitters to increase the SNR and, hence, the communication range.

Our results show that the LED arrays outperform single-LED transmitters, offering a higher SNR due to the smaller FOV of their elements. Additionally, it is demonstrated that different geometries of arrays achieve varying levels of improvement. In particular, the honeycomb hexagonal array provides the furthest communication distance, achieving a 19% increase compared to the single-LED transmitter.

The remainder of this paper is organized as follows: Section 2 presents the theoretical background of calculating the SNR. Section 3 presents the geometry of the proposed V2V communication system, MATLAB [40] simulation parameters, and modeling of the square-, single hexagonal-, octagonal-, and honeycomb hexagonal-shaped LED array transmitter (Tx) configurations. Section 4 compares the irradiance distributions of the proposed LED arrays at a 1 m distance. Section 5 evaluates the SNR performance across different design parameters and compares the SNR results of the proposed transmitters. Section 6 presents a discussion, and Section 7 outlines the theoretical and practical implications of the study. Finally, Section 8 concludes the paper.

2. Theoretical Background

This section presents the required formulas to model the V2V VLC system scenario in MATLAB. The system consists of two LED transmitters, Tx1 and Tx2, and a photodiode receiver, Rx. The transmitted light signal is OOK-modulated. The signal travels through the channel and reaches the receiver. For simplicity, we assume the LEDs to be Lambertian emitters with a certain FOV. In addition, we assume that only additive white Gaussian noise (AWGN) is present in the system, and ignore effects such as weather conditions, air turbulence, ambient noise from sunlight, and multipath fading.

Instantaneous transmitted power from a Lambertian emitter can be written as [41]

$$X(\phi, t) = X(\phi)e^{j\omega t} \tag{1}$$

where ϕ is the angle of irradiance, ω is the angular frequency, and

$$X(\phi) = X_0 \cos^m(\phi) \tag{2}$$

where m is the order of the Lambertian emission:

$$m = -\frac{\ln(2)}{\ln(\cos(\phi_{\frac{1}{2}}))} \tag{3}$$

and $\phi_{\frac{1}{2}}$ is the transmitter's half FOV.

The output signal $Y(t)$ of an optical wireless channel can be expressed as [41]

$$Y(t) = \gamma X(t) \otimes h(t) + N(t) \tag{4}$$

where γ represents the photodetector responsivity, $h(t)$ is the impulse response, \otimes denotes convolution, and $N(t)$ is the AWGN.

The average transmitter power is calculated as follows [5]:

$$P_t = \frac{1}{T} \int_0^T X(t) dt \tag{5}$$

where $T = \frac{2\pi}{\omega}$ is the period.

Once P_t is known, the received power can be calculated by [5]

$$P_r = H(0)P_t \tag{6}$$

where $H(0) = \int_{-\infty}^{\infty} h(t) dt$ is the DC channel gain, which is given by [5]

$$H(0) = \begin{cases} \frac{(m+1)A}{2\pi D^2} \cos^m(\phi) T_s(\psi) g(\psi) \cos(\psi), & 0 \leq \psi \leq \psi_c \\ 0, & \text{otherwise} \end{cases} \tag{7}$$

where A is the area of the photodetector, D is the distance between the transmitter and receiver, ϕ is the angle of irradiance, ψ is the angle of incidence, $T_s(\psi)$ is the signal transmission coefficient of an optical filter, $g(\psi)$ is the gain of the optical concentrator, and ψ_c is the receiver's half FOV.

The gain achieved by an idealized concentrator with an internal refractive index n is given by [5]

$$g(\psi) = \begin{cases} \frac{n^2}{\sin^2(\psi_c)}, & 0 \leq \psi \leq \psi_c \\ 0, & \text{otherwise} \end{cases} \tag{8}$$

The SNR represents the performance quality of a given channel. The signal component is given by [41]

$$S = \gamma^2 P_{rSignal}^2 \tag{9}$$

where

$$P_{rSignal} = \frac{1}{T} \int_0^T \left(\sum_{i=1}^{LEDs} h_i(t) \otimes X(t) \right) dt \tag{10}$$

The Gaussian noise is the sum of the contributions from shot noise, thermal noise, and intersymbol interference due to an optical path difference. The total variance N is given as [41]

$$N = \sigma_{shot}^2 + \sigma_{thermal}^2 + \gamma^2 P_{rISI}^2 \tag{11}$$

where

$$P_{rISI} = \lim_{T' \rightarrow \infty} \frac{1}{T' - T} \int_T^{T'} \left(\sum_{i=1}^{LEDs} h_i(t) \otimes X(t) \right) dt \tag{12}$$

The shot noise and thermal noise contributions are given as [41]

$$\sigma_{shot}^2 = 2qR \left(P_{Signal} + P_{r,ISI} \right) B_{en} + 2qI_{bg} I_2 B_{en} \tag{13}$$

$$\sigma_{thermal}^2 = \frac{8\pi k T_k}{G} \delta A I_2 B_{en}^2 + \frac{16\pi^2 k T_k E}{g_m} \delta^2 A^2 I_3 B_{en}^3 \tag{14}$$

where q is the electron charge, B_{en} is the equivalent noise bandwidth, I_{bg} is the background current, I_2 is the noise bandwidth factor, k is the Boltzmann's constant, T_k is the absolute temperature, G is the open-loop voltage gain, δ is the fixed capacitance of the photodetector per unit area, E is the field-effect transistor (FET) channel noise factor, g_m is the FET transconductance, $I_3 = 0.0868$, and $P_{r,ISI}$ is the power received through intersymbol interference.

Once the shot and thermal noise contributions are known, the SNR is calculated as follows: [41]

$$\text{SNR} = \frac{S}{N} \tag{15}$$

The BER for OOK modulation can be calculated using [5]

$$\text{BER} = Q\left(\sqrt{\text{SNR}}\right) \tag{16}$$

where

$$Q(x) = \frac{1}{2\pi} \int_x^\infty e^{-y^2/2} dy \tag{17}$$

Equations (2) and (3) are used to plot the irradiance distribution from the two transmitters of the modeled VLC system. Then, Equations (6), (7), (9) and (11)–(15) are utilized to simulate the SNR of the VLC system against distance. Finally, the BER is plotted against distance using Equations (16) and (17).

3. Approach and Methodology

The VLC system considered in this paper has two transmitters, Tx1 and Tx2, which are the taillights of the vehicle traveling in front of another vehicle carrying a photodiode receiver, as illustrated in Figure 1. L_1 is the distance between Tx1 and Rx, and L_2 is the distance between Tx2 and Rx.

From Equations (3) and (7), it is known that when the LED transmitter of a VLC system has a narrow FOV, its Lambertian emission coefficient (m) increases, resulting in a larger DC channel gain $H(0)$. However, vehicle taillights are designed with wide FOVs. To address this, we employ LED arrays of various geometrical shapes, where each individual LED has a narrow FOV. This approach allows the array transmitters to illuminate the same area as a wide-FOV LED while benefiting from the narrow FOVs of each LED.

LED arrays are commonly used in vehicle headlights and taillights. For instance, Figure 2 presents Samsung’s PixCell LED headlight design, which features a light-emitting surface that is just 1/16 the size of a traditional one, making it one of the smallest lighting solutions in the automotive industry. The design incorporates 4 rows of 100 LEDs in total, covering an area of 15.4 mm × 2.74 mm [42].

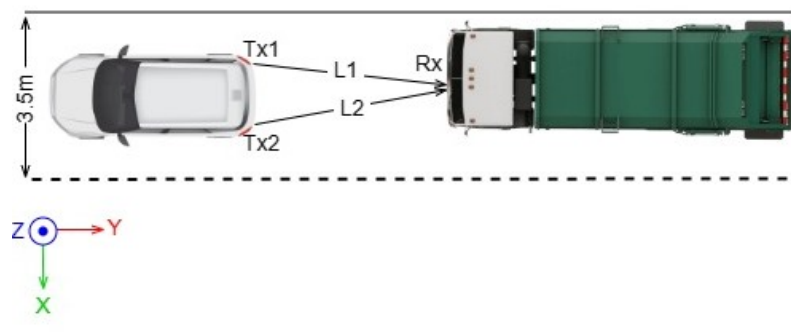


Figure 1. The road scenario for the proposed vehicle-to-vehicle (V2V) system.

To evaluate the effect of using LED arrays as transmitters in a V2V VLC system on system performance, we consider six different configurations. The first one, established as a reference, uses two single LEDs with power P_0 for each transmitter, Tx1, and Tx2. The irradiance distribution provided by these transmitters in the plane $y = 1$ m serves as the reference. All the proposed LED array configurations are intended to yield this reference irradiance distribution in the plane $y = 1$ m.

The second configuration has 3 × 3 square LED arrays, with each LED in the transmitter array having a power of $P_0/9$. The third configuration uses single hexagonal-shaped arrays consisting of 9 LEDs, each with a power of $P_0/9$. The fourth configuration has

octagonal array transmitters, again consisting of 9 LEDs each with a power of $P_0/9$. Since these three configurations have the same number of LEDs, it will be possible to observe the difference in system performance resulting from the geometry of the LED arrays.

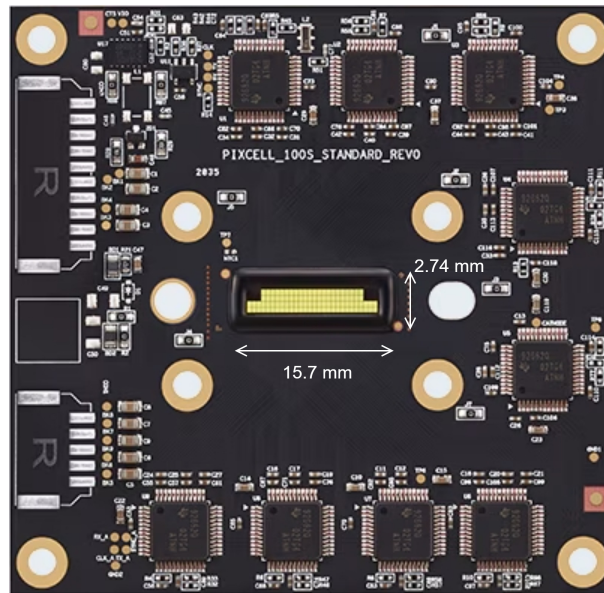


Figure 2. Samsung’s PixCell LED headlight module [42].

Additionally, the fifth configuration has 5×5 square LED arrays, with each LED having a power of $P_0/25$. Finally, the last one has honeycomb-like hexagonal arrays consisting of 25 LEDs. Again, each LED has a power of $P_0/25$. Since the geometries of the 3×3 and 5×5 square array transmitters are the same except for the number of elements, it will be possible to evaluate the effect of increasing the number of elements and, thus, the size of the array on system performance. Furthermore, by comparing the fifth and sixth configurations, we can determine whether using a more complex geometry than a simple square, hexagon, or octagon has any advantage in terms of system performance.

In Figure 1, the vehicles are traveling in the negative y direction. The separation between the transmitters, Tx1 and Tx2, is fixed at $D = 1.5$ m, their height from the road is 70 cm, and the lane width is 3.5 m. The midpoint between the transmitters is selected as the origin. The transmitter and receiver coordinates are given in Table 1. The coordinates show that the receiver has a 75 cm lateral misalignment from each transmitter, but no vertical misalignment.

Table 1. Transmitter and receiver coordinates.

| Component | X (cm) | Y (cm) | Z (cm) |
|-----------|--------|--------|--------|
| Tx1 | −75 | 0 | 0 |
| Tx2 | 75 | 0 | 0 |
| Rx | 0, 350 | y | 0, 30 |

4. The Geometries of the Proposed Transmitters

4.1. The Geometry for the Single-LED Transmitter Case

Since the distance between the two taillights is 150 cm, the two transmitters of the single-LED configuration are located at $P(\pm 75 \text{ cm}, 0, 0)$. Each transmitter is a single LED with a half FOV ϕ_1 of 30° . Their power is focused in a circular area of radius $R = d \tan \phi_1$ in the plane $y = d$, where d is the y -location of Rx. The power drops to half its maximum

value at the boundary of this circle. At a particular y -distance d , the two circles will be tangent. This distance is found to be $d = 130$ cm using

$$2d \tan(\phi_1) = 150 \text{ cm} \tag{18}$$

The geometry of the single-LED transmitter case is illustrated in Figure 3.

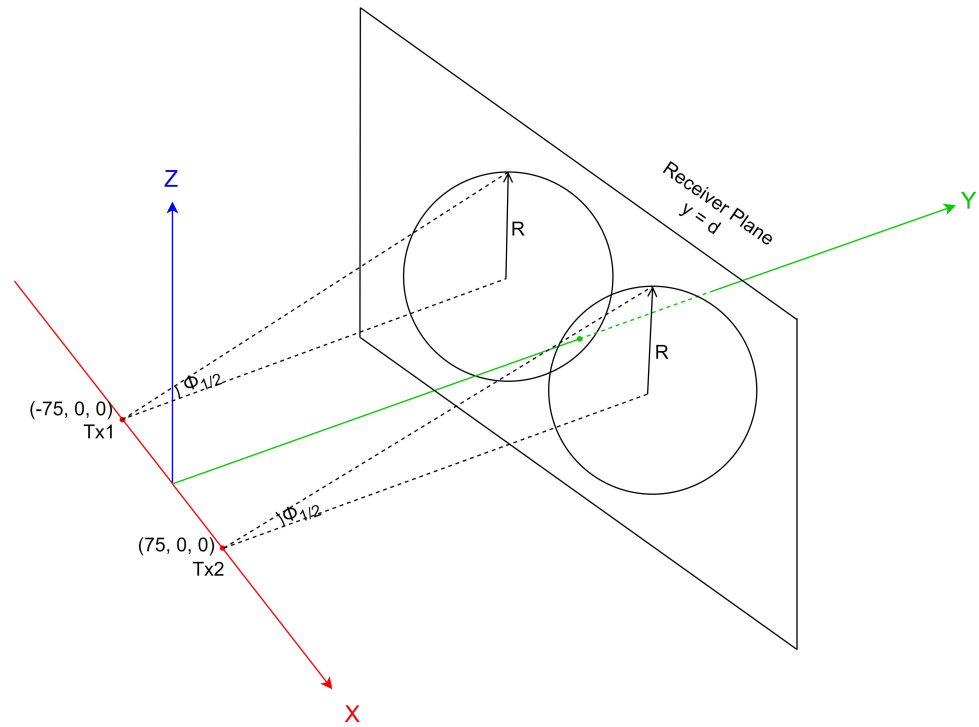


Figure 3. The geometry for the single light-emitting diode (LED) case.

4.2. 3 × 3 Square Array

As depicted in Figure 4, a square LED array of size 3 × 3 with a spacing of s is proposed, where s is initially set to 1 cm. This value was chosen arbitrarily, and it will be shown later that variations in s do not significantly impact system performance. Each LED element, denoted as $e_{i,j}$, has a field of view of $\phi'_{1/2}$, and is aligned along an orientation vector $\mathbf{O}_{i,j}$, with each vector intersecting the $y = d_0$ plane at point $e'_{i,j}$, where d_0 is a design parameter. The $y = d_0$ plane is defined as the plane on which the two arrays formed by the points $e'_{i,j}$ from the two transmitters are tangent, as shown in Figure 5. In other words, the outermost points of the two arrays intersect each other. For this condition to be met, the elements $e'_{i,j}$ should be separated by $D/2$ on this plane. The naming convention for the array elements is illustrated in the matrix below.

$$\begin{bmatrix} e_{1,1} & e_{1,0} & e_{1,-1} \\ e_{0,1} & e_{0,0} & e_{0,-1} \\ e_{-1,1} & e_{-1,0} & e_{-1,-1} \end{bmatrix} \tag{19}$$

The location of the element $e_{i,j}$ relative to the center element $e_{0,0}$ is given by $P(sj, 0, si)$. To achieve the geometry illustrated in Figure 4, the orientation vector $\mathbf{O}_{i,j}$ with starting point $P(sj, 0, si)$ (location of $e_{i,j}$) should intersect the $y = d_0$ plane at $P(\frac{D}{2}j, d_0, \frac{D}{2}i)$ (location of $e'_{i,j}$). Thus, the required vector can be found using

$$\mathbf{O}_{i,j} = \langle (\frac{D}{2} - s)j, d_0, (\frac{D}{2} - s)i \rangle \tag{20}$$

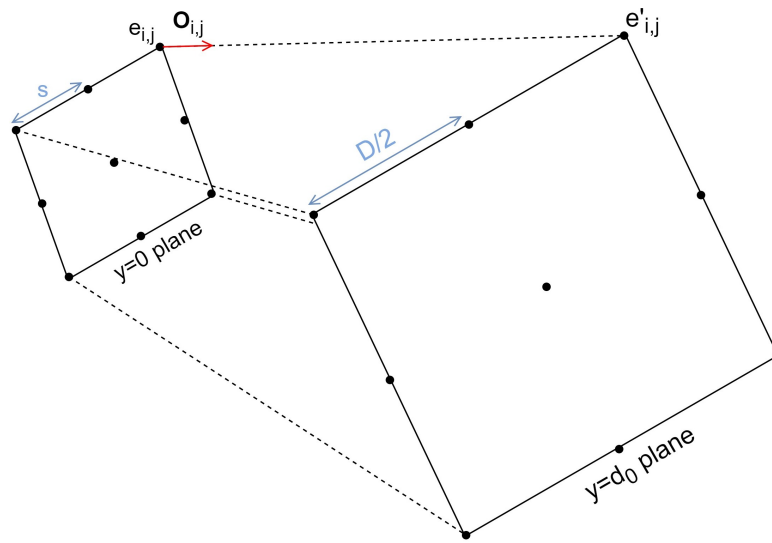


Figure 4. The 3 × 3 square-shaped LED array geometry.

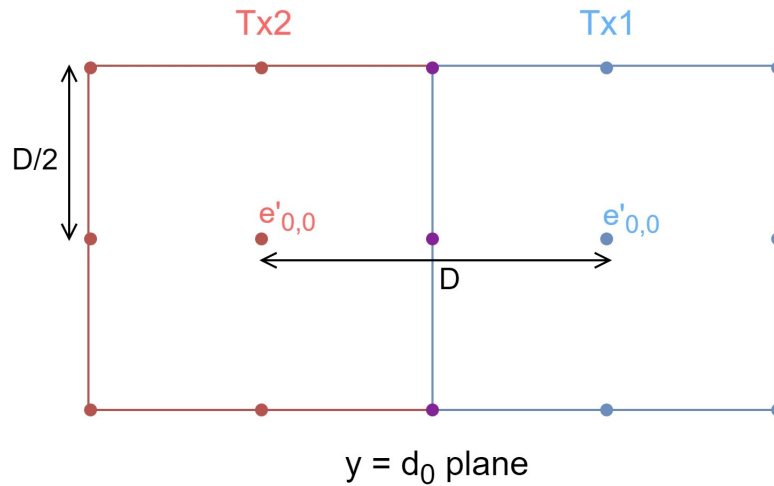


Figure 5. The 3 × 3 square arrays formed by the points $e'_{i,j}$ on the $y = d_0$ plane.

The reason why the distance d_0 and half FOV $\phi'_{\frac{1}{2}}$ are determined as the design parameters is that a narrower half FOV $\phi'_{\frac{1}{2}}$ yields a larger SNR, and the value of d_0 conveniently adjusts the orientation vectors (refer to Equation (20)) of the LEDs in the array. The orientation vectors are crucial since the taillights of a vehicle are essentially used for lighting purposes, not as transmitters in the communication link. Therefore, we need to ensure that they can illuminate a certain area.

We assume that each of the two LEDs, one for Tx1 and one for Tx2, in the single-LED case has a power P_0 and an intensity I_0 . To keep the power dissipation of both proposed transmitter configurations at the same level, the power of each LED in the square array transmitter is determined as $P_0/9$. Since the intensity is proportional to the power level divided by the squared tangent of the half FOV, the intensity I_1 of each LED of the 3 × 3 square array is set as follows:

$$I_1 = \frac{1}{9} \frac{\tan^2 \phi_{\frac{1}{2}}}{\tan^2 \phi'_{\frac{1}{2}}} I_0 \tag{21}$$

The initial values of the design parameters for the two transmitters are listed in Table 2. The design parameter d_0 is set at 130 cm, which is equal to the y -distance where the

two circles illustrated in Figure 3 become tangent (found to be 130 cm using Equation (18)). Using Equations (2) and (3), and the values given in Table 2, the irradiance distributions in the plane $y = 1$ m are plotted using MATLAB software for the two proposed configurations. The results are given in Figure 6a,b.

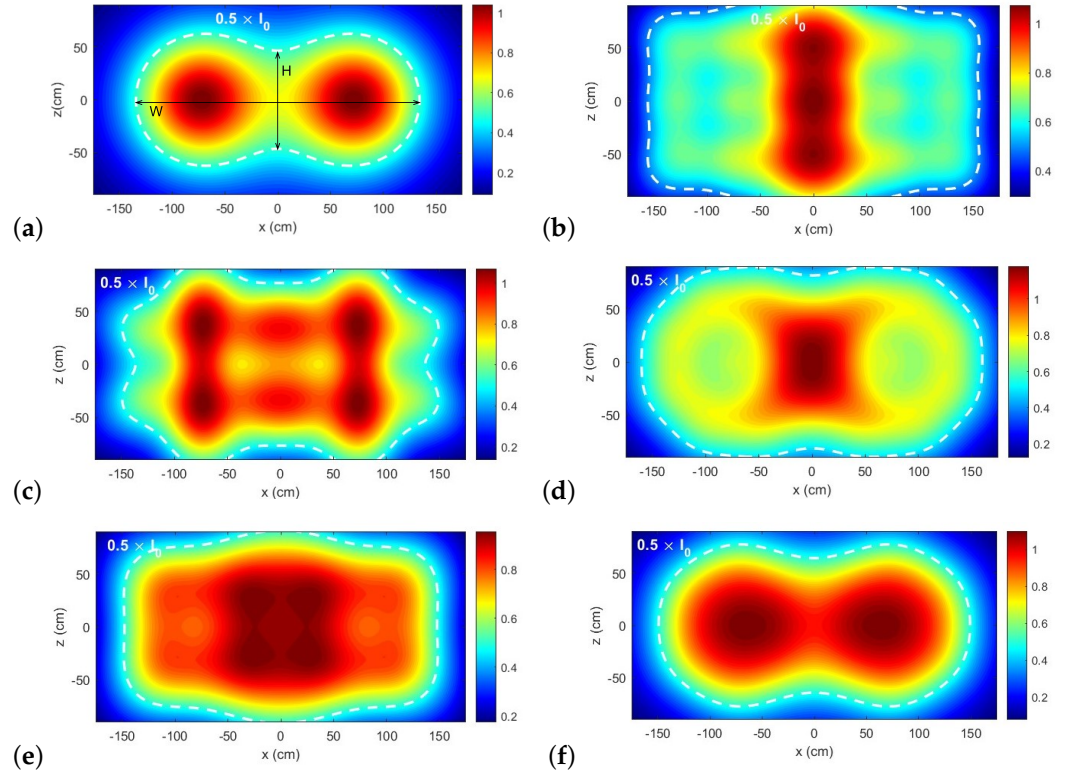


Figure 6. Irradiance distributions at $y = 1$ m with $d_0 = 130$ cm: (a) with the single-LED transmitters, (b) with the 3×3 square array transmitters, (c) with the single hexagonal array transmitters, (d) with the octagonal array transmitters, (e) with 5×5 square array transmitters, and (f) with the honeycomb hexagonal array transmitters.

Table 2. The initial values of the design parameters for the single-LED and square array cases.

| Parameter | Value |
|-----------------------|------------|
| s | 1 cm |
| D | 150 cm |
| P_0 | 10 W |
| $\phi_{\frac{1}{2}}$ | 30° |
| I_0 | 1 |
| d_0 | 130 cm |
| $\phi'_{\frac{1}{2}}$ | 15° |
| I_1 | 0.52 |
| I_2 | 0.52 |
| I_3 | 0.52 |
| I_4 | 0.18 |
| I_5 | 0.18 |

4.3. Single Hexagonal Array

As shown in Figure 7, a single hexagonal-shaped array transmitter is proposed with separation s between each individual LED. Each LED $e_{i,j}$ has a half FOV $\phi'_{\frac{1}{2}}$ and is oriented along a vector $\mathbf{O}_{i,j}$ crossing the location of $e_{i,j}$ at $y = 0$ plane and the location of $e'_{i,j}$ on the $y = d_0$ plane (illustrated in Figure 8). Similar to the 3×3 square array case, the $y = d_0$

plane is defined such that the two arrays formed by the points $e'_{i,j}$ from the two transmitters become tangent, as illustrated in Figure 9. To meet this condition, the separation between the $e'_{i,j}$ points should be $D/\sqrt{3}$. With the naming convention of Figure 7, the locations of elements $e_{i,j}$ and $e'_{i,j}$ relative to the center element $e_{0,0}$ are determined with

$$P(s\frac{\sqrt{3}}{2}j, 0, s\frac{1}{2}i) \tag{22}$$

and

$$P(\frac{D}{N}\frac{\sqrt{3}}{2}j, d_0, \frac{D}{N}\frac{1}{2}i) \tag{23}$$

respectively.

Thus, the required orientation vectors $\mathbf{O}_{i,j}$ can be calculated by

$$\langle (\frac{D}{\sqrt{3}} - s)\frac{\sqrt{3}}{2}j, d_0, (\frac{D}{\sqrt{3}} - s)\frac{1}{2}i \rangle \tag{24}$$

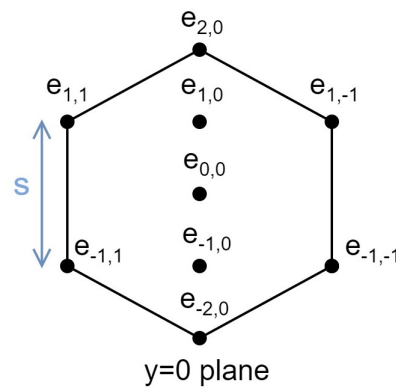


Figure 7. Single hexagonal-shaped array geometry.

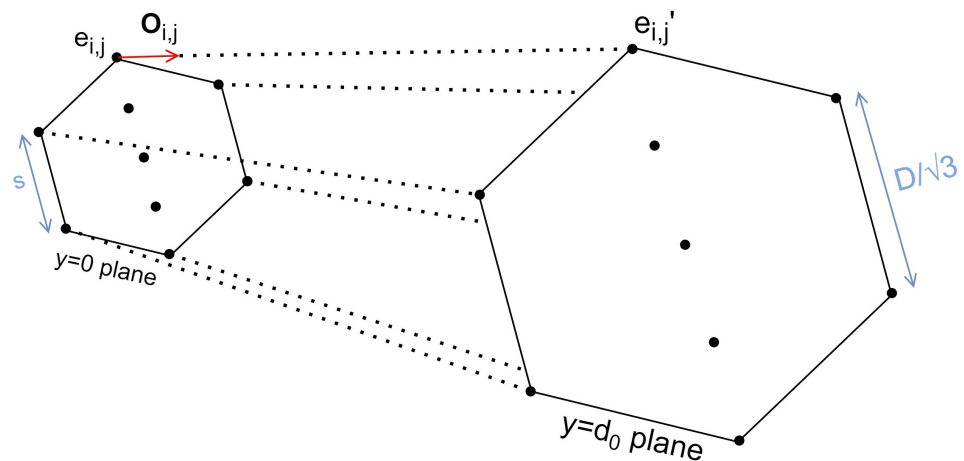


Figure 8. Single hexagonal-shaped array geometry and orientation vectors.

The power of each LED in the single hexagonal array transmitter is determined to be $P_0/9$ since it includes a total of nine LEDs. Proportional to the power level divided by the squared tangent of the half FOV, the intensity I_2 of each LED of the single hexagonal array is set as follows:

$$I_2 = \frac{1}{9} \frac{\tan^2 \phi_{\frac{1}{2}}}{\tan^2 \phi'_{\frac{1}{2}}} I_0 \tag{25}$$

The initial values of the design parameters for the single hexagonal array are listed in Table 2. Using Equations (2) and (3), and the values given in Table 2, the irradiance

distribution on the plane $y = 1$ m is plotted using MATLAB. The result is presented in Figure 6c.

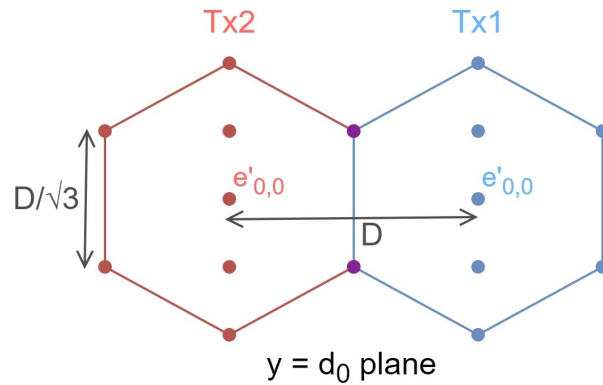


Figure 9. Single hexagonal arrays formed by the points $e'_{i,j}$ on the $y = d_0$ plane.

4.4. Octagonal Array

As shown in Figure 10, an octagonal-shaped array transmitter is proposed with a separation s between each LED. Each element has a half FOV of $\phi'_{\frac{1}{2}}$. Again, each LED $e_{i,j}$ is oriented along a vector $\mathbf{O}_{i,j}$ crossing the location of the $e_{i,j}$ at $y = 0$ plane and the location of $e'_{i,j}$ on the $y = d_0$ plane. Consistently throughout all configurations, the $y = d_0$ plane is defined such that the two octagonal arrays formed by the $e'_{i,j}$ points from the two transmitters become tangent on this plane (illustrated in Figure 11). To meet this condition, the separation between the $e'_{i,j}$ points should be $D/(\sqrt{2} + 1)$.

With the naming convention of Figure 10, the locations of the elements $e_{i,j}$ and $e'_{i,j}$ relative to the center element $e_{0,0}$ are determined with

$$P\left(\frac{s}{2}j, 0, s\frac{\sqrt{2} + 1}{4}i\right), \quad i = \text{even}; \tag{26}$$

$$P\left(s\frac{\sqrt{2} + 1}{2}j, d_0, \frac{s}{2}i\right), \quad i = \text{odd}. \tag{27}$$

and

$$P\left(\frac{D}{2(\sqrt{2} + 1)}j, d_0, \frac{D}{4}i\right), \quad i = \text{even}; \tag{28}$$

$$P\left(\frac{D}{2}j, d_0, \left(\frac{D}{2(\sqrt{2} + 1)}i\right)\right), \quad i = \text{odd}. \tag{29}$$

respectively.

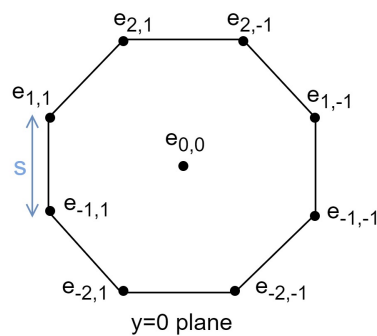


Figure 10. Octagonal -shaped LED array geometry.

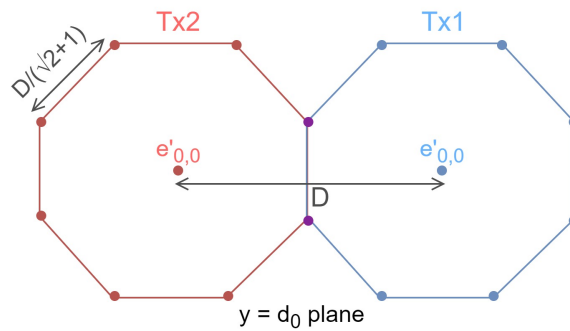


Figure 11. Octagonal arrays formed by the $e'_{i,j}$ points on the $y = d_0$ plane.

Thus, the required orientation vectors $\mathbf{O}_{i,j}$ can be calculated by

$$\langle (\frac{D}{\sqrt{2}+1} - s)\frac{j}{2}, d_0, (\frac{D}{\sqrt{2}+1} - s)\frac{\sqrt{2}+1}{4}i \rangle, \quad i = \text{even}; \tag{30}$$

$$\langle (\frac{D}{\sqrt{2}+1} - s)\frac{\sqrt{2}+1}{2}j, d_0, (\frac{D}{\sqrt{2}+1} - s)\frac{i}{2} \rangle, \quad i = \text{odd}. \tag{31}$$

Similar to the considerations made for the 3×3 square array and the single hexagonal array, the power of each LED in the octagonal array transmitter is determined to be $P_0/9$ since it includes a total of nine LEDs. Proportional to the power level divided by the squared tangent of the half FOV, the intensity I_3 of each LED of the array is set as follows:

$$I_3 = \frac{1}{9} \frac{\tan^2 \phi_{\frac{1}{2}}}{\tan^2 \phi'_{\frac{1}{2}}} I_0 \tag{32}$$

The initial values of the design parameters for the octagonal array are listed in Table 2. Using Equations (2) and (3), and the values given in Table 2, the irradiance distribution in the plane $y = 1$ m is plotted using MATLAB software. The result is given in Figure 6d.

4.5. 5×5 Square-Shaped Array

As depicted in Figure 12, a square LED array of size 5×5 with a spacing of s is proposed, where s is set to 1 cm. Each LED element, denoted as $e_{i,j}$, has a field of view of $\phi'_{\frac{1}{2}}$ and is aligned along an orientation vector $\mathbf{O}_{i,j}$, with each vector intersecting the $y = d_0$ plane at a point $e'_{i,j}$. Similar to the other configurations, the $y = d_0$ plane is defined such that the two square arrays formed by the $e'_{i,j}$ points from the two transmitters become tangent on this plane (illustrated in Figure 13). To meet this condition, the separation between the $e'_{i,j}$ points should be $D/4$. The naming convention for the array elements is illustrated in the matrix below.

$$\begin{bmatrix} e_{2,2} & e_{2,1} & e_{2,0} & e_{2,-1} & e_{2,-2} \\ e_{1,2} & e_{1,1} & e_{1,0} & e_{1,-1} & e_{1,-2} \\ e_{0,2} & e_{0,1} & e_{0,0} & e_{0,-1} & e_{0,-2} \\ e_{-1,2} & e_{-1,1} & e_{-1,0} & e_{-1,-1} & e_{-1,-2} \\ e_{-2,2} & e_{-2,1} & e_{-2,0} & e_{-2,-1} & e_{-2,-2} \end{bmatrix} \tag{33}$$

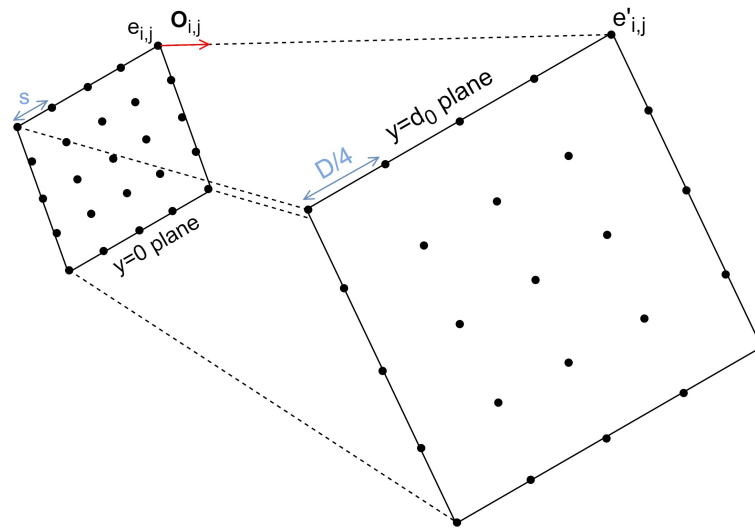


Figure 12. Square-shaped LED array geometry.

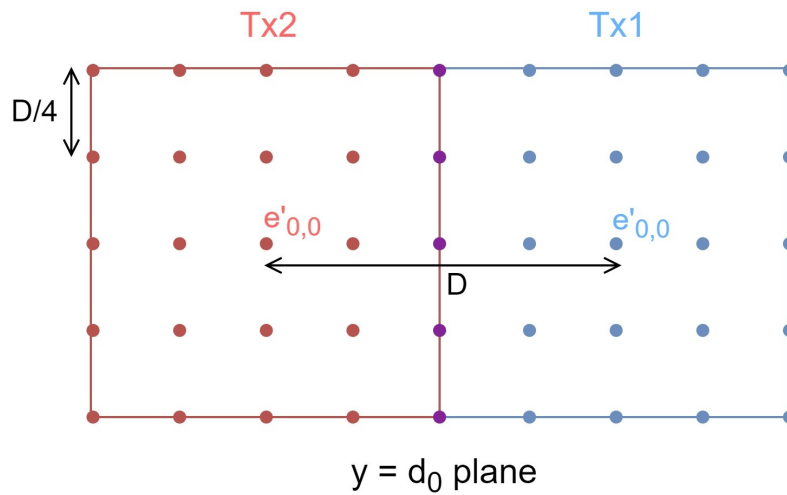


Figure 13. 5×5 square arrays formed by the $e'_{i,j}$ points on the $y = d_0$ plane.

The location of the element $e_{i,j}$ relative to the center element $e_{0,0}$ is given by $P(sj, 0, si)$. To achieve the geometry illustrated in Figure 12, the orientation vector $\mathbf{O}_{i,j}$ with starting point $P(sj, 0, si)$ (location of $e_{i,j}$) should intersect the $y = d_0$ plane at $P(\frac{D}{4}j, d_0, \frac{D}{4}i)$ (location of $e'_{i,j}$). Thus, the required vector can be found using

$$\mathbf{O}_{i,j} = \langle (\frac{D}{4} - s)j, d_0, (\frac{D}{4} - s)i \rangle \tag{34}$$

The power of each LED in the square array transmitter is determined to be $P_0/25$. Since the intensity is proportional to the power level divided by the squared tangent of the half FOV, the intensity I_4 of each LED of the square array is set as follows:

$$I_4 = \frac{1}{25} \frac{\tan^2 \phi'_2}{\tan^2 \phi'_1} I_0 \tag{35}$$

The initial values of the design parameters for the two transmitters are listed in Table 2. Using Equations (2) and (3), and the values given in Table 2, the irradiance distribution in the plane $y = 1$ m is plotted using MATLAB. The result is given in Figure 6e.

4.6. Honeycomb Hexagonal Array

As shown in Figure 14, a honeycomb-shaped hexagonal array transmitter is proposed with a separation s between each LED. Each element has a half FOV of $\phi'_{\frac{1}{2}}$. Again, each LED $e_{i,j}$ is oriented along a vector $\mathbf{O}_{i,j}$ crossing the location of $e_{i,j}$ on the $y = 0$ plane and the location of $e'_{i,j}$ on the $y = d_0$ plane. Consistently, the $y = d_0$ plane is defined such that the two honeycomb hexagonal arrays formed by the $e'_{i,j}$ points from the two transmitters become tangent on this plane (illustrated in Figure 15). To meet this condition, the separation between the $e'_{i,j}$ points should be $D/5$.

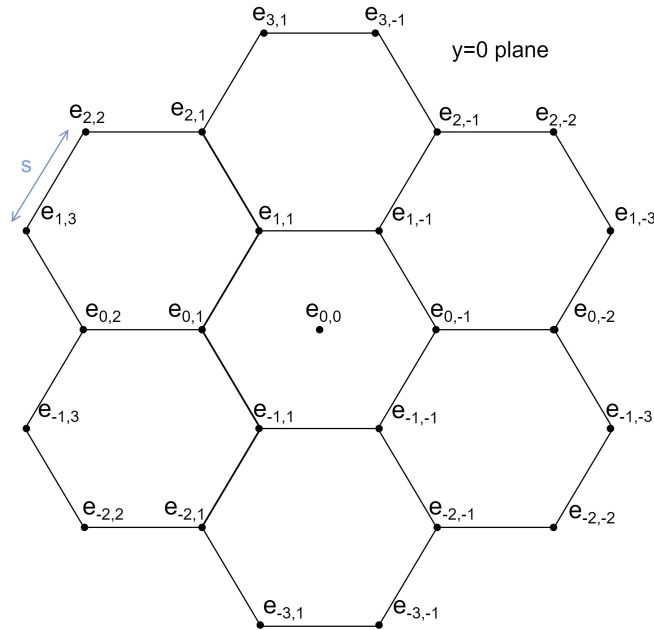


Figure 14. Honeycomb hexagonal-shaped array geometry.

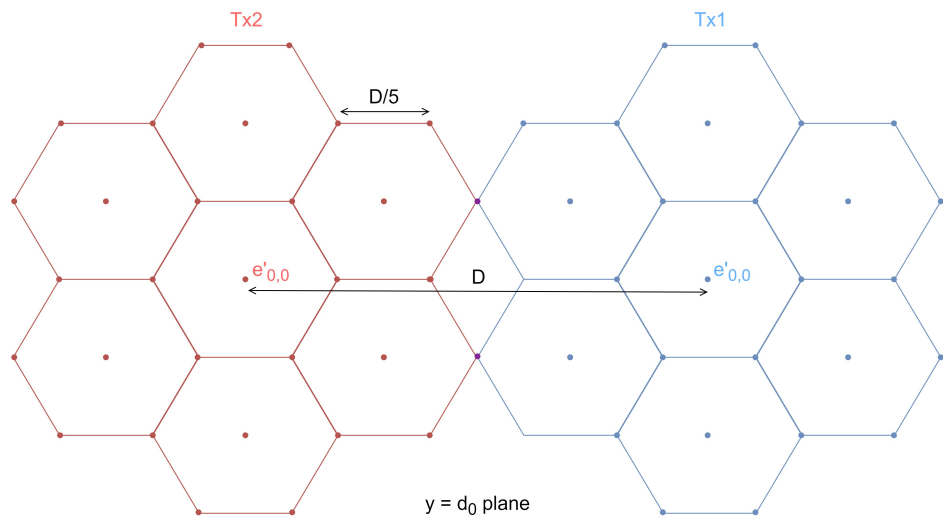


Figure 15. Honeycomb hexagonal arrays formed by the $e'_{i,j}$ points on the $y = d_0$ plane.

With the naming convention of Figure 14, the locations of the elements $e_{i,j}$ and $e'_{i,j}$ relative to the center element $e_{0,0}$ are determined with

$$P(sj, 0, s\frac{\sqrt{3}}{2}i), \quad i = \text{even}; \tag{36}$$

$$P(s \operatorname{sign}(j)(|j| - 0.5), d_0, s \frac{\sqrt{3}}{2}i), \quad i = \text{odd}. \tag{37}$$

and

$$P(\frac{D}{N}j, d_0, \frac{D}{N} \frac{\sqrt{3}}{2}i), \quad i = \text{even}; \tag{38}$$

$$P(\frac{D}{N} \operatorname{sign}(j)(|j| - 0.5), d_0, \frac{D}{N} \frac{\sqrt{3}}{2}i), \quad i = \text{odd}. \tag{39}$$

respectively.

Thus, the required orientation vectors $\mathbf{O}_{i,j}$ can be calculated by

$$\langle (\frac{D}{N} - s)j, d_0, (\frac{D}{N} - s) \frac{\sqrt{3}}{2}i \rangle, \quad i = \text{even}; \tag{40}$$

$$\langle (\frac{D}{N} - s) \operatorname{sign}(j)(|j| - 0.5)j, d_0, (\frac{D}{N} - s) \frac{\sqrt{3}}{2}i \rangle, \quad i = \text{odd}. \tag{41}$$

Similar to the considerations made for the other arrays, the power of each LED in the honeycomb hexagonal array transmitter is determined to be $P_0/25$ since it includes a total of 25 LEDs. Proportional to the power level divided by the squared tangent of the half FOV, the intensity I_5 of each LED of the array is set as follows:

$$I_5 = \frac{1}{25} \frac{\tan^2 \phi_{\frac{1}{2}}}{\tan^2 \phi'_{\frac{1}{2}}} I_0 \tag{42}$$

The initial values of the design parameters for the honeycomb hexagonal array are listed in Table 2. Using Equations (2) and (3), and the values given in Table 2, the irradiance distribution on the plane $y = 1$ m is plotted using MATLAB software. The result is given in Figure 6f.

Established as a reference, we take the irradiation distribution of the single-LED transmitters at $y = 1$ m, which is shown in Figure 6a. An area with an irradiance of at least 0.5 is considered illuminated. The height of the illuminated area is given as H , and the width as W , as shown in Figure 6a. We aim to keep the values of H and W equal for all the configurations so that the illuminated areas remain approximately the same.

As seen in Figure 6, all the array transmitters manage to illuminate the area that is illuminated by the reference configuration of single-LED transmitters. The H and W values for the different configurations are given in Table 3. The array transmitters illuminate larger areas compared to the single LEDs with a current value of d_0 . Therefore, we can adjust the value of d_0 to enhance the system performance as long as the H and W values do not become smaller than those of the single-LED transmitters.

Table 3. H and W values for the six configurations, where $d_0 = 130$ cm for all the array geometries.

| Configuration | H (cm) | W (cm) |
|---------------------|--------|--------|
| Single-LED | 92 | 268 |
| 3 × 3 square | >180 | 310 |
| Single hexagonal | 152 | 272 |
| Octagonal | 162 | 320 |
| 5 × 5 square | >180 | 296 |
| Honeycomb hexagonal | 128 | 298 |

5. Results

5.1. SNR Performance with Different Values of Design Parameters

The design parameters for a given array with separation s are the half FOV $\phi'_{\frac{1}{2}}$ and the distance d_0 . As explained earlier, d_0 is the distance at which the two arrays formed by the

points $e'_{i,j}$, which are the points where the orientation vectors of the two array transmitters intersect the plane $y = d_0$, from the two transmitters are tangent to each other.

We expect a higher SNR with a decreasing half FOV $\phi'_{\frac{1}{2}}$ since the DC channel gain is proportional to the Lambertian coefficient m (refer to Equation (7)), whereas m is inversely proportional to the half FOV $\phi'_{\frac{1}{2}}$ (refer to Equation (3)). In the proposed array transmitter configurations, this relationship is exploited to enhance the SNR by using LEDs with smaller half FOVs. To validate our expectation, we chose two of the proposed configurations and plotted the SNR against distance y in MATLAB with different values of $\phi'_{\frac{1}{2}}$. The simulation parameters are listed in Table 4.

Table 4. Simulation parameters and values.

| Parameter | Value |
|---|--|
| Modulation scheme | OOK |
| Modulation frequency | 1 MHz |
| Receiver area A | 1 cm ² |
| Optical filter gain T_s | 1 |
| Optical concentrator gain g | 10 |
| Transmitted power P_t | 10 W |
| Transmitter half FOV $\phi_{\frac{1}{2}}$ | 30° |
| Array transmitter half FOV $\phi'_{\frac{1}{2}}$ | 15° |
| Receiver responsivity γ | 0.54 A/W |
| Receiver FOV ψ_c | 60° |
| Boltzmann's constant k | 1.3806488 × 10 ⁻²³ J/K |
| Absolute temperature T_k | 300 K |
| Fixed capacitance of photodetector per unit area δ | 1.12 × 10 ⁻¹⁰ F/cm ² |
| Noise bandwidth factor I_2 | 0.562 |
| I_3 | 0.0868 |
| Noise bandwidth B | 10 ⁸ Hz |
| Open-loop voltage gain G | 10 |
| FET channel noise factor E | 1.5 |
| FET transconductance g_m | 3 × 10 ⁻² S |
| Electron charge q | 1.6 × 10 ⁻¹⁹ C |
| Background current I_{bg} | 5.1 × 10 ⁻³ A |
| Photodiode dark current I_0 | 10 ⁻⁸ A |

Figure 16 shows the SNR vs. distance for the 5 × 5 square array and the octagonal array with $d_0 = 130$ and $\phi'_{\frac{1}{2}} = 15^\circ, 30^\circ, \text{ and } 45^\circ$. As expected, we observe that the SNR increases as the half FOV decreases. Therefore, the proposed LED array transmitter configurations are expected to yield a higher SNR than the reference configuration with single-LED transmitters, since the single LEDs have a half FOV of $\phi_{\frac{1}{2}} = 30^\circ$, whereas the LEDs in the array transmitter have a narrower half FOV of $\phi'_{\frac{1}{2}} = 15^\circ$.

We expect the SNR to increase with d_0 because the orientation vectors of the array make smaller angles with the y-axis as d_0 increases (refer to Equations (20), (24), (30), (31), (34), (40) and (41)). Therefore, the light from each LED falls on the receiver with smaller angles of irradiance ϕ , which results in higher DC channel gain $H(0)$, as seen from Equation (7).

Since the value of d_0 should affect all the array geometries similarly, two of the proposed array transmitter configurations are selected and the SNR is plotted versus distance y in MATLAB with different values of d_0 to validate our expectation. Figure 17 shows the SNR versus distance for the 5 × 5 square array and the octagonal array with $d_0 = 130$ cm, 160 cm, and 190 cm. We observe that the SNR increases with d_0 , which validates our expectation. The same result is expected for the other transmitter configurations, as well.

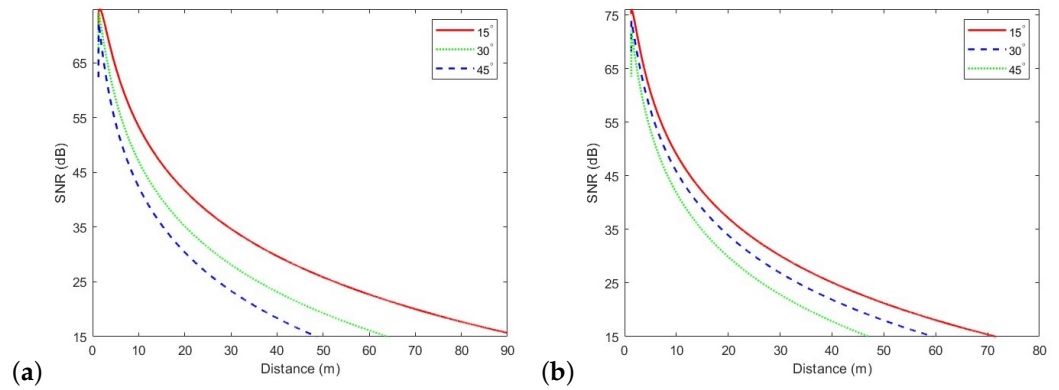


Figure 16. Signal-to-noise ratio (SNR) vs. distance plots with $d_0 = 130$ cm and $\phi'_{\frac{1}{2}} = 15^\circ, 30^\circ,$ and 45° : (a) for the 5×5 square array transmitters and (b) for the octagonal array transmitters.

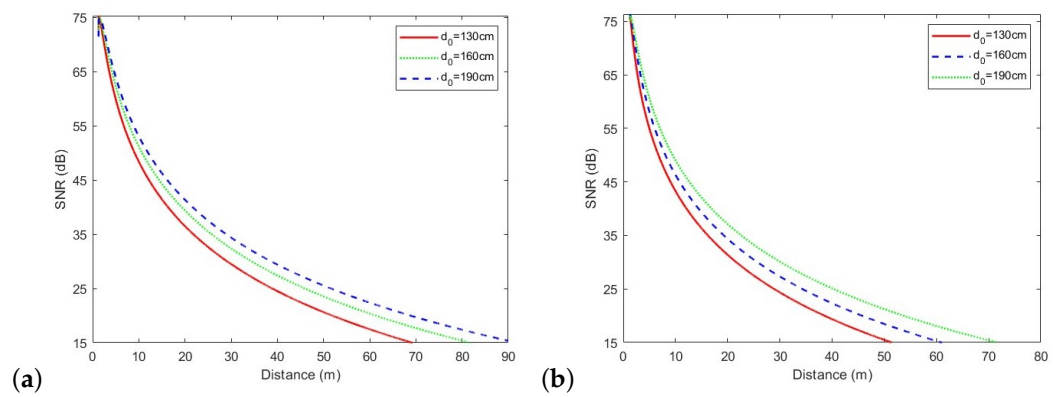


Figure 17. SNR vs. distance plots for the square array with $\phi'_{\frac{1}{2}} = 15^\circ$ and $d_0 = 130, 160,$ and 190 cm: (a) for the 5×5 square array transmitters and (b) for the octagonal array transmitters.

Since a larger value of d_0 is required for enhanced system performance, the final values of the design parameter d_0 are maximized while ensuring the H and W values are never smaller in any array geometry than those of the single-LED transmitters. The final values are determined and listed in Table 5. The irradiance distributions of each configuration at $y = 1$ m with these final values are given in Figure 18, and the H and W values for each configuration are given in Table 6. It is seen that we can ensure that a desired area is illuminated by a particular LED array geometry by properly adjusting the value of d_0 .

Table 5. The final values of the design parameters.

| Parameter | 3 × 3 Square | Single Hexagonal | Octagonal | 5 × 5 Square | Honeycomb Hexagonal |
|-----------------------|--------------|------------------|------------|--------------|---------------------|
| $\phi'_{\frac{1}{2}}$ | 15° | 15° | 15° | 15° | 15° |
| d_0 | 230 cm | 187 cm | 193 cm | 196 cm | 160 cm |
| Power | 1.11 W/LED | 1.11 W/LED | 1.11 W/LED | 0.4 W/LED | 0.4 W/LED |

Table 6. The H and W values for the six configurations with the final values of d_0 .

| Configuration | H | W |
|---------------------|----|-----|
| Single-LED | 92 | 268 |
| 3 × 3 square | 92 | 280 |
| Single hexagonal | 92 | 278 |
| Octagonal | 92 | 292 |
| 5 × 5 square | 92 | 280 |
| Honeycomb hexagonal | 92 | 286 |

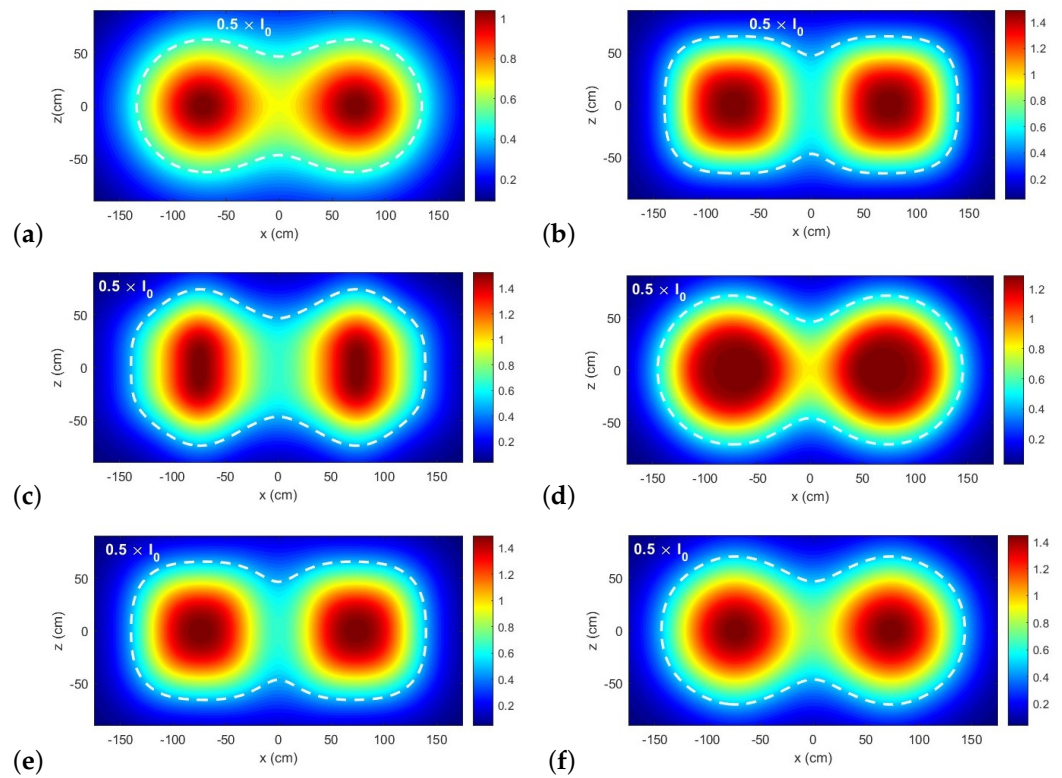


Figure 18. The irradiance distributions at $y = 1$ m with the final values of the design parameters: (a) with the single-LED transmitters, (b) with the 3×3 square array transmitters, (c) with the single hexagonal array transmitters, (d) with the octagonal array transmitters, (e) with 5×5 square array transmitters, and (f) with the honeycomb hexagonal array transmitters.

5.2. SNR Performances of Proposed Transmitters

Figure 19 shows SNR vs. distance curves for each proposed transmitter. As expected, the SNR decreases with distance for all the transmitter configurations. According to the IEEE 802.15.7 standard [43], the minimum acceptable SNR level is 15 dB and the maximum acceptable BER is 10^{-6} . Therefore, we considered a communication range with a minimum SNR level of 15 dB. We observe that the distance achievable with this limit is between 70 and 85 m. It is seen that the array transmitters have improved performance compared to the single-LED transmitter system. The communication ranges for each transmitter are given in Table 7. We find that the honeycomb hexagonal array transmitters offer the longest communication range. Specifically, they achieve a 19% longer range than the one provided by the single-LED transmitters.

Table 7. The communication ranges of the proposed transmitter configurations at a 15 dB signal-to-noise ratio (SNR) threshold.

| Transmitter Type | Range |
|---------------------------|--------|
| Single-LED | 70.5 m |
| 3×3 square array | 78.7 m |
| Single hexagonal array | 78.6 m |
| Octagonal array | 72.7 m |
| 5×5 square array | 80.1 m |
| Honeycomb hexagonal array | 83.8 m |

Figure 19 shows that the array geometries including a larger number of LEDs provide longer communication ranges. Including 25 LEDs, the 5×5 square and honeycomb

hexagonal array transmitters have a higher SNR than the 3×3 square, single hexagonal, and octagonal arrays that include 9 LEDs.

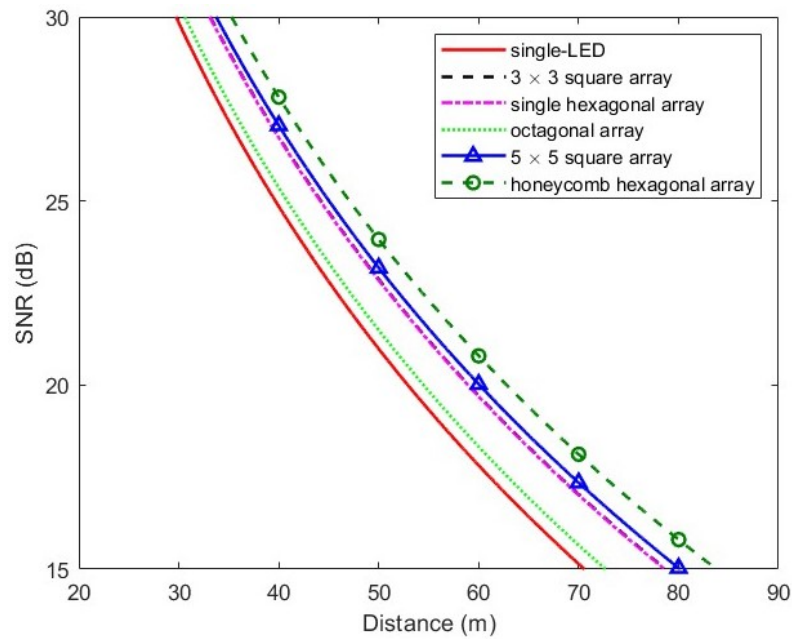


Figure 19. An SNR vs. distance plot for the proposed transmitters.

To understand why the honeycomb hexagonal arrays outperformed the 5×5 square arrays, despite both having the same number of LEDs, we need to examine their geometries closely. Each LED in the array transmitters has a half FOV of 15° , while the transmitter must still illuminate the same area as a 30° half FOV LED. We adjusted the LED orientations to satisfy this requirement. The orientation vector $\mathbf{O}_{0,0}$ of the center LED $e_{0,0}$ is aligned with the y-axis. In contrast, the orientation vectors of the surrounding LEDs are angled relative to the y-axis. As a result, the light from these LEDs hits the receiver at steeper angles of irradiance, reducing the DC channel gain $H(0)$ (refer to Equation (7)). When an LED is closer to the center LED, its orientation vector becomes less angled with the y-axis, resulting in a narrower angle of irradiance. In the honeycomb hexagonal array, the distances between the center LED and adjacent LEDs are shorter than those in the 5×5 square array, leading to a higher SNR in the honeycomb array.

Since there are as few as nine LEDs in the 3×3 square, single hexagonal, and octagonal array transmitters, the orientation vectors of each array make larger angles with the y-axis. In contrast, the 5×5 square and honeycomb hexagonal arrays include 25 LEDs, allowing their inner LEDs to have more moderate angles with the y-axis. Moreover, the 3×3 square arrays, with nine LEDs, performed better than the other two nine-LED arrays due to their advantage in illuminating the region between the transmitters, $-75 \text{ cm} < x < 75 \text{ cm}$. When d_0 decreases below a certain value, the LED arrays tend to fail in illuminating this region. The 3×3 square array can sustain a larger d_0 before failing to illuminate the middle region because, as seen in Figure 5, the 3×3 square array has six LEDs, three from each transmitter, aimed towards the middle region. Thus, it can illuminate the desired area with a larger value of d_0 , which results in less steep orientation vectors, causing this configuration to perform better than the single hexagonal and octagonal arrays. Finally, the single hexagonal array outperformed the octagonal array because its elements are closer together near the center, again allowing for less angled orientation vectors.

Initially, the receiver was misaligned horizontally by 75 cm from each transmitter, Tx1 and Tx2, with zero vertical misalignment. To assess the impact of misalignment on system performance across the six proposed configurations, we plotted the SNR against distance

with the receiver positioned at $P(350 \text{ cm}, y, 30 \text{ cm})$. After this adjustment, the misalignment of the receiver was as follows:

- **From Tx1:**
 - Horizontal: 425 cm
 - Vertical: 30 cm
- **From Tx2:**
 - Horizontal: 275 cm
 - Vertical: 30 cm

As expected, Figure 20 shows that all of the six configurations perform worse when the misalignment is more severe. Nevertheless, the array transmitter configurations still outperform the single-LED transmitters.

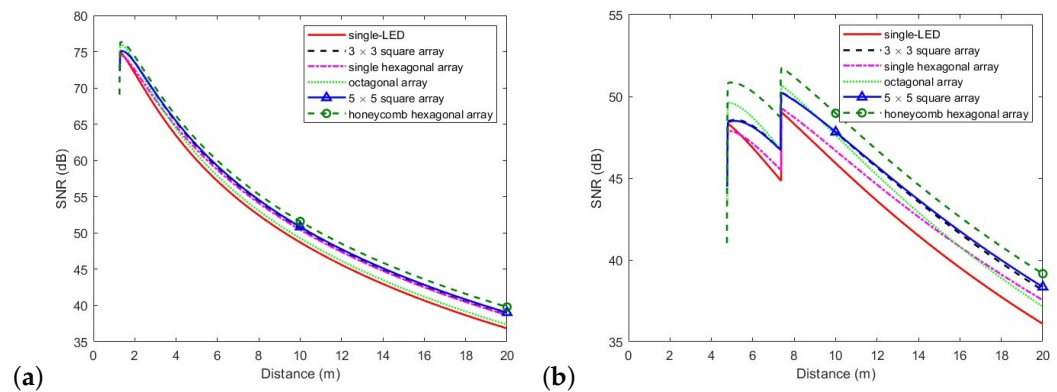


Figure 20. SNR vs. distance for the proposed transmitters in the short range: (a) with the initial receiver position and (b) with the receiver positioned at $P(350 \text{ cm}, y, 30 \text{ cm})$.

Although we expected poorer system performance with more severe misalignment, we do not anticipate any performance change in the long range. This is because the vectors from Tx1 and Tx2 to the receiver will deviate by very small angles when the distance is large, making the receiver appear to the transmitters as if its location did not change. The dominant factor limiting system performance is the long distance between the transmitters and the receiver. Figure 21 validates our expectation, showing that the results with the new misalignment conditions are almost identical to the results with the initial misalignment conditions.

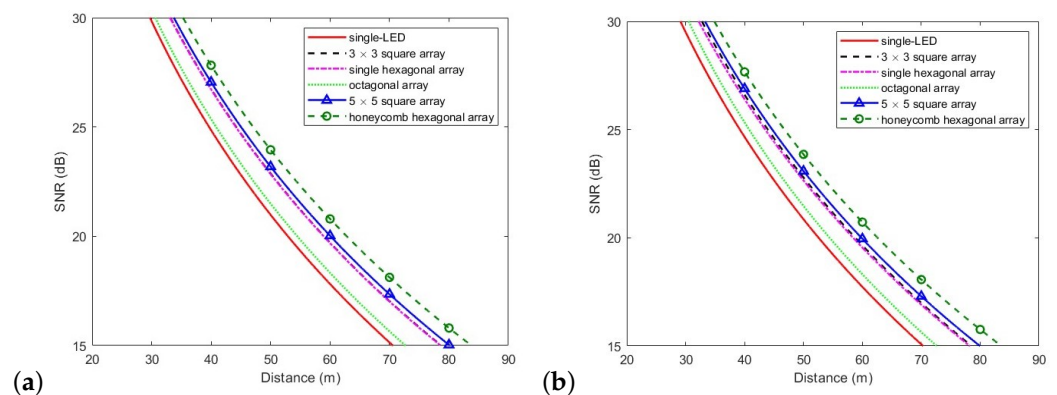


Figure 21. SNR vs. distance for the proposed transmitters in the long range: (a) with the initial receiver position and (b) with the receiver positioned at $P(350 \text{ cm}, y, 30 \text{ cm})$.

The BER of the VLC system is computed using Equations (16) and (17), and it is plotted against the SNR, as depicted in Figure 22. It is observed that the BER becomes

10^{-6} at 13.2 dB SNR. This result suggests that the system achieves a BER lower than the maximum acceptable level specified in the IEEE 802.15.7 standard [43] at 15 dB SNR, which was chosen as the minimum SNR threshold for determining the communication ranges.

In Figure 23, the BER for the six proposed transmitter configurations is plotted against distance. As expected, the BER increases with distance for all transmitter configurations. The distances at which the BER reaches 10^{-6} are given in Table 8. Notably, the honeycomb hexagonal transmitters achieve a 19% improvement compared to the single-LED transmitters.

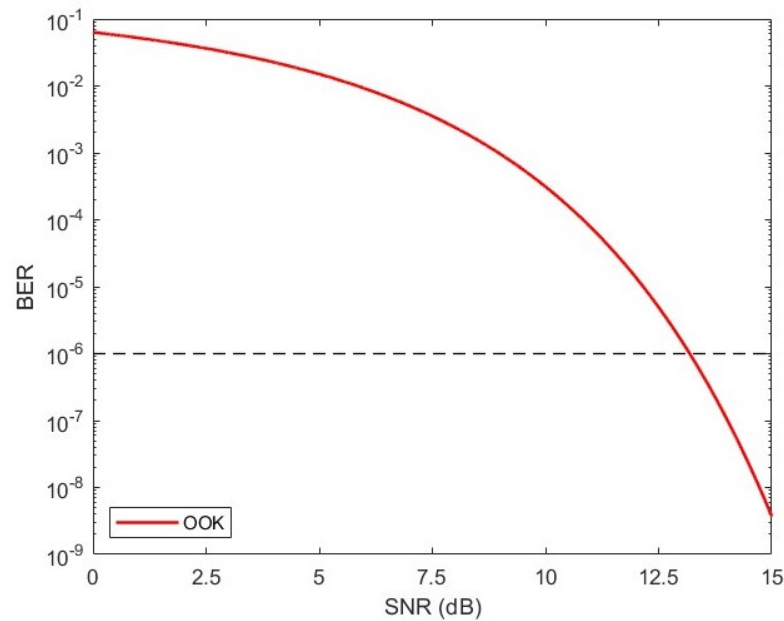


Figure 22. A BER vs. SNR plot for the communication link.

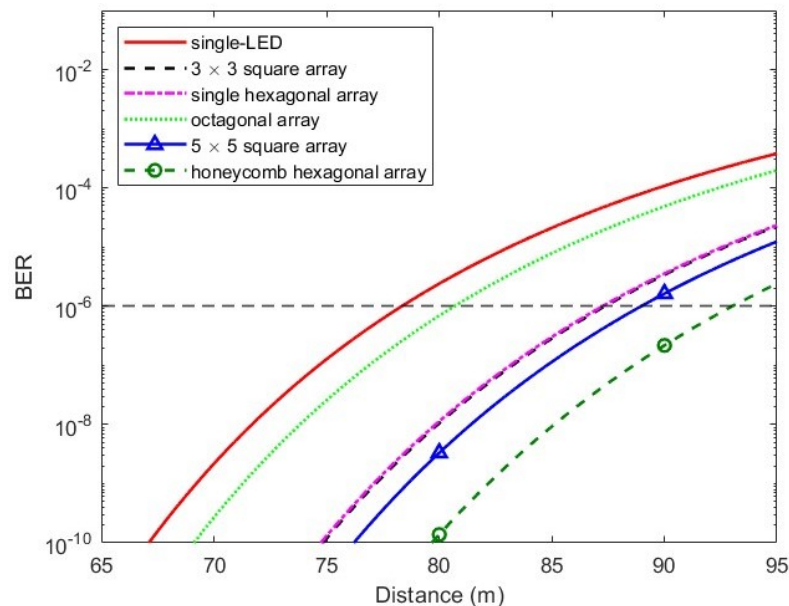


Figure 23. A bit error rate (BER) vs. distance plot for the proposed transmitters.

To assess the design’s ease of implementation in the automotive industry, we compare the size of our transmitter designs to that of Samsung’s PixCell LED module, shown in Figure 2, as this module has a light-emitting surface that is 1/16 the size of a traditional one. When we decrease the value of s while keeping d_0 constant, we expect more angled orientation vectors, though we do not anticipate significant deterioration in system performance.

To validate this prediction, simulations were conducted with s decreased from 1 cm to 1 mm. With this change, our largest LED array, the honeycomb hexagonal array, covers an area of 5 mm \times 5 mm, which is even smaller than Samsung’s PixCell LED module. As shown in Figure 24, these results are similar to those in Figure 19 for $s = 1$ cm. The communication ranges for each transmitter are provided in Table 9 for $s = 1$ mm. We observe that the honeycomb hexagonal array transmitters offer a 16% improvement in system performance, which remains robust even with such a compact light-emitting surface.

Table 8. The distances at which the bit error rate (BER) reaches 10^{-6} for the proposed transmitter configurations.

| Transmitter Type | Range |
|---------------------------|--------|
| Single-LED | 78.4 m |
| 3 \times 3 square array | 87.4 m |
| Single hexagonal array | 87.3 m |
| Octagonal array | 80.7 m |
| 5 \times 5 square array | 89.0 m |
| Honeycomb hexagonal array | 93.0 m |

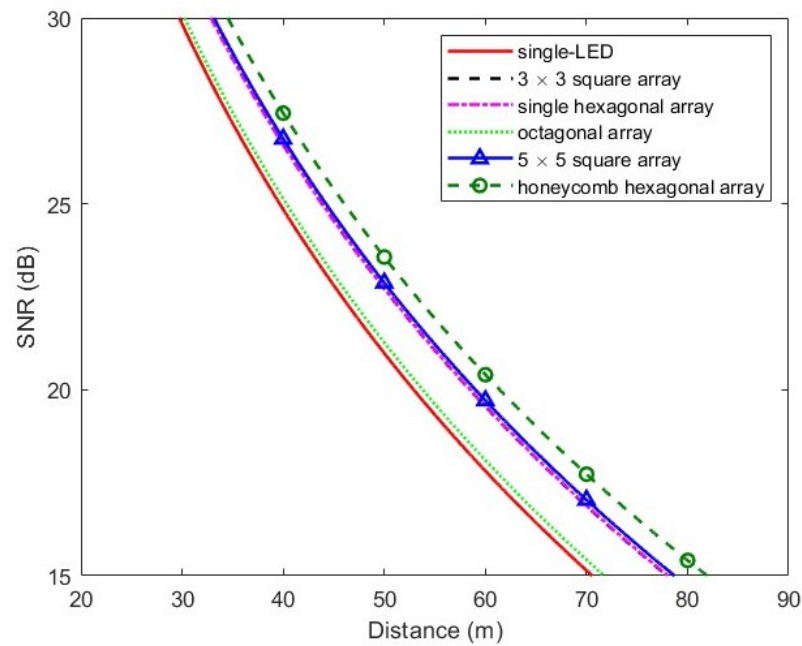


Figure 24. An SNR vs. distance plot for the proposed transmitters with the value of s decreased to 1 mm.

Table 9. The communication ranges of the proposed transmitter configurations with s decreased to 1 mm, evaluated at a 15 dB SNR threshold.

| Transmitter Type | Range |
|---------------------------|--------|
| Single-LED | 70.5 m |
| 3 \times 3 square array | 78.0 m |
| Single hexagonal array | 78.0 m |
| Octagonal array | 71.7 m |
| 5 \times 5 square array | 78.7 m |
| Honeycomb hexagonal array | 81.9 m |

Therefore, our design offers flexibility in the choice of spacing s , as it mainly affects the orientation vector angles, while system performance remains robust even with very small values of s . These results remain consistent as long as d_0 is kept constant. This allows

automotive manufacturers to adjust the design of lighting equipment to meet specific size or aesthetic requirements.

6. Discussion

In this paper, we established a reference configuration using a single-LED transmitter and plotted its irradiance distribution at a short distance, specifically at $y = 1$ m. Subsequently, we proposed various LED array geometries with two design parameters: the half FOV ϕ'_1 of each LED and d_0 . We examined the effect of each design parameter by plotting the SNR against distance for the square array transmitters with different values of ϕ'_1 , and then different values of d_0 . The results showed that the SNR increases as ϕ'_1 decreases and d_0 increases. By appropriately adjusting the design parameters, we achieved the reference irradiance distribution with all configurations while extending the communication range. This demonstrates that our method allows for obtaining the desired irradiance pattern by adjusting the orientation vectors of the LEDs, controlled by the value of d_0 , and the half FOV for each LED, thereby improving the SNR.

In [37], the irradiance and SNR distributions of an indoor VLC system are compared for different configurations of an LED array consisting of 16 LEDs. The paper proposes three different arrangements. The first is a regular 4×4 square array with equal spacing between the LEDs. The second and third configurations include the same number of LEDs; however, the arrangement of the LEDs is different. The paper shows that their second and third models yield more uniform irradiance and SNR distributions throughout the room.

On the other hand, in this study, we used LED arrays to alter the system performance as desired. Therefore, we aimed to increase the SNR rather than achieve uniformity. For a V2V VLC system, a uniform SNR across a plane at a certain distance is not required. Instead, a long communication range is preferred, which is not required for an indoor VLC system. By using different configurations of LED arrays, we achieved an increased communication distance while maintaining the desired irradiance pattern.

The study in [31] aims to increase the communication distance of a V2V VLC system by overdriving the LED transmitter current and proportionally shortening the duration of the pulses. Although the study in [31] tried to reduce the duty cycles of the signals and keep the overall irradiance constant, the instantaneous irradiance of the LEDs in these short signals may pose a danger to human eye health. Unlike [31], in our study, the current and, naturally, the irradiance were kept constant, and the communication distance was increased by simply changing the geometric structures of the LED arrays.

In [30], the irradiance distribution is shown from a top view, covering both lateral and longitudinal aspects. Our paper, however, offers a more comprehensive approach by plotting the irradiance distribution directly on the plane where the receiver is located, thus including both lateral and ground clearance. The study in [30] includes a comparison of day and night conditions, as well. We assumed clear weather conditions in our simulations; however, the exact compatibility of our chosen parameters with real conditions is not a concern, as our study serves as a proof of concept. On the contrary, this approach enhances the flexibility of our study and its applicability to various scenarios.

The study in [35] presents SNR and distance graphs using square pixel photodiode arrays in the receiver to extend the communication range. In contrast, our paper improves the VLC performance by optimizing the transmitter side without enlarging the receiver. Additionally, in [35], simulations with different modulation schemes are conducted, with the transmitted power adjusted according to the needs of each scheme. In contrast, our study maintains a constant transmitted power of 10 W across all proposed transmitter configurations, achieving increased communication ranges without varying the power.

Our goal is to offer new LED arrays that will increase the communication potential of V2V VLC systems in terms of SNR and communication distance, in addition to existing headlights and taillights that meet the standards set by the automotive industry. Therefore, rather than relying on existing light output schemes, our study investigates how these

schemes can be optimized for communication. In addition, LED arrays are designed in this paper to increase the received power rather than reduce the background noise. In arrays with better performance, the received power is larger and the background noise is higher, as expected from the shot noise formula given in Equation (13). However, since the received power is higher, the SNR values of these arrays are also better.

The literature comprehensively examines different transmitter LED configurations in indoor VLC systems. However, in indoor studies, the LED arrays are usually used for the purpose of yielding a uniform SNR throughout the room. No literature for indoor studies aims to increase the communication range, as this is unnecessary for indoor applications. In addition, existing outdoor studies for increasing the SNR and communication range in V2V VLC focus on optimizing the receiver side. This paper aims to increase the SNR value and communication range of V2V VLC systems by changing the geometry of the LED arrays on the transmitter side. In addition, in indoor studies, the LED configurations are varied only through the arrangement of the locations of the LEDs. However, we adjust the orientations of the LEDs as well to provide the same effective FOV throughout different geometries. We establish a reference configuration that has an FOV of 60° , and we design LED arrays where each LED has a 30° FOV, yet we manage to ensure that every configuration illuminates approximately the same area. This approach allows us to more accurately reflect the actual performance of different LED configurations and exploit the smaller FOV of these LEDs to increase the communication range and SNR. Therefore, this paper gives an insight into how to optimize system performance by increasing the SNR and communication range of V2V VLC systems by changing the geometry of the LED array transmitters and the orientations of each LED.

In addition, while existing studies in the literature generally deal with a limited number of LED configurations, our paper uses six transmitter configurations, bringing a new perspective to the literature by developing a unique analysis methodology with a wide range of LED configurations with different orientations of LEDs, revealing the potential of new structures that can be used especially in outdoor V2V VLC systems. In particular, the honeycomb-shaped hexagonal array and the octagonal array configurations do not exist in the literature, and we examine the effects of these structures on the SNR and communication distance in detail. In fact, our newly used honeycomb-shaped hexagonal configuration gave the best SNR and communication distance. In this context, our study makes a significant contribution to the existing literature.

7. Theoretical and Practical Implications

This study presents a new approach by comparing different geometric LED array configurations, focusing on SNR and BER performances in V2V systems. From a theoretical perspective, this study provides fundamental insights into the impact of varying LED geometries (such as honeycomb, hexagonal, octagonal, and square arrays) on the efficiency and communication range of VLC systems. Our theoretical comparisons show that the honeycomb array provides the best SNR performance, with a communication range improvement of 19% at 1 cm spacing and 16% at a 1 mm spacing, compared to a single-LED setup, indicating that geometry plays an important role in maximizing communication performance under ideal conditions. Our study also highlights how geometric optimization can be used to improve communication systems without changing the total power of LED arrays.

From a practical perspective, this research provides a solid foundation for future experimental studies. It is suggested that adapting LED array geometries has the potential to improve V2V communication systems. Although the focus is on simulation data, it provides a theoretical framework for comparing different arrays in outdoor environments. This has the capacity to improve V2V communication performance, especially in scenarios of high-speed vehicles. It is a fact that even a few centimeters of communication distance gain in traffic will speed up access to critical data and enable drivers or autonomous systems to make quick decisions. For example, according to studies conducted by the

National Highway Traffic Safety Administration (NHTSA), even millisecond delays can cause an increase in accidents [44]. The increase in communication distance provided by the honeycomb array can increase safety between vehicles by providing more reliable data transmission during critical time periods.

We demonstrated that our proposed transmitter design performs robustly even when the sizes of the LED arrays are decreased drastically. We reduced the sizes of the LED arrays such that our largest array is smaller than one of the smallest industrial headlight modules, Samsung's PixCell LED [42,45]. This result emphasizes the versatility of our design, which not only adapts well to compact dimensions, but also allows automotive manufacturers the flexibility to tailor lighting solutions to meet their specific size and aesthetic requirements while ensuring effective communication ranges.

8. Conclusions

V2V VLC is a promising technology for improving traffic safety and efficiency, particularly during high-traffic periods. However, it is challenging to achieve a high SNR over long communication distances. In the literature, most of the papers that address this problem are focused on the receiver side, whereas few studies are focused on the transmitter. Therefore, this paper is focused on optimizing the VLC transmitter to address this problem. The use of different arrangements of LED arrays has been studied for indoor VLC systems to achieve a uniform SNR throughout the room. In this paper, we demonstrate that LED arrays can also be beneficial for outdoor VLC systems by increasing the SNR, and consequently, the communication range.

This paper investigated various LED array geometries by first establishing a reference configuration using single-LED transmitters and plotting its irradiance distribution at $y = 1$ m. Different LED array geometries were then proposed with two key design parameters: the half FOV $\phi'_{\frac{1}{2}}$ of each LED and d_0 .

Subsequently, we examined the performance of square array transmitters with varying $\phi'_{\frac{1}{2}}$ and d_0 values, noting that decreasing $\phi'_{\frac{1}{2}}$ and increasing d_0 enhance the SNR and, hence, extend the communication range. We then adjusted these design parameters for each proposed transmitter geometry, aiming to minimize $\phi'_{\frac{1}{2}}$ and maximize d_0 while ensuring that all the proposed transmitters have the same irradiance distributions at $y = 1$ m.

From a theoretical perspective, system performance improves as the value of d_0 increases or the FOV of the LEDs decreases without bound. However, the design imposes the constraint that the illuminated height (H) and width (W) must remain constant. Consequently, the values of these parameters are limited. Their values were carefully selected to optimize system performance while maintaining consistent H and W dimensions across all designs.

Additionally, the separation distance (s) between the LEDs in the array presents another design constraint. While increasing the array size generally enhances performance, a more compact design is preferable for practical headlight or taillight modules. This creates a trade-off between maximizing system performance and minimizing the overall physical dimensions of the module.

With these conditions met, we fixed the design parameters and plotted the SNR against distance for all transmitter configurations. The results consistently showed that the LED arrays outperformed single-LED transmitters, primarily due to the smaller FOV of their elements. For a 15 dB SNR threshold and a separation of $s = 1$ cm, the communication ranges were determined to be 70.5 m for single-LED transmitters, 78.7 m for 3×3 square array transmitters, 78.6 m for single hexagonal transmitters, 72.7 m for octagonal transmitters, 80.1 m for 5×5 square array transmitters, and 83.8 m for honeycomb hexagonal array transmitters. Notably, the honeycomb hexagonal transmitters achieved the longest communication distance, yielding a 19% increase compared to the single-LED transmitters.

Furthermore, we plotted the BER against the SNR and found that the BER reached 10^{-6} at an SNR of 13.2 dB. In addition, a plot of BER versus distance for all the transmitter

configurations was produced and the distances where the BER becomes 10^{-6} were found to be 78.4 m for the single-LED transmitters, 87.4 m for the 3×3 square array transmitters, 87.3 m for the single hexagonal array transmitters, 80.7 m for the octagonal array transmitters, 89.0 m for the 5×5 square array transmitters, and 93.0 m for the honeycomb hexagonal array transmitters.

In addition, we demonstrated that our proposed transmitter design performs robustly even when the sizes of the LED arrays are decreased drastically. The honeycomb hexagonal transmitter design provided a 19% improvement in system performance with a spacing of 1 cm, which slightly decreased to 16% when the spacing was reduced to 1 mm, a change that also made the array size 100 times smaller. Despite this reduction, its performance remains commendable, especially since, at $s = 1$ mm, our largest array is smaller than one of the smallest industrial headlight modules, Samsung's PixCell LED. This result emphasizes the versatility of our design, which not only adapts well to compact dimensions but also allows automotive manufacturers the flexibility to tailor lighting solutions to meet their specific size and aesthetic requirements while ensuring effective communication ranges.

These findings highlight the effectiveness of optimizing the half FOV ϕ'_1 and the orientation vectors, controlled by d_0 , of each LED in the array transmitters. Our method allows for achieving the desired irradiance patterns and optimizing communication ranges across different transmitter configurations.

This study shows the critical role of adjusting the geometrical configuration of the transmitter LED array in optimizing VLC performance. Future research should explore further optimizations of LED arrays and assess the impact of dynamic environmental conditions on system performance. Such work may include validating simulation results with experimental data and conducting more comprehensive analyses related to real-life conditions. The performances of different LED arrays in outdoor conditions, such as different weather conditions like smoky and foggy atmospheres, can be examined to provide data for real-world applications. In this regard, future experimental studies can be compared with our simulation-based analysis, with external weather factors included, to make important contributions to the development of LED-based communication systems.

Author Contributions: Conceptualization, A.D., M.O. and H.Y.; methodology, A.D., M.O. and H.Y.; software, A.D. and M.O.; validation, A.D., M.O. and H.Y.; formal analysis, A.D., M.O. and H.Y.; investigation, A.D., M.O. and H.Y.; resources, A.D., M.O. and H.Y.; data curation, A.D. and M.O.; writing—original draft preparation, A.D. and M.O.; writing—review and editing, A.D., M.O. and H.Y.; visualization, A.D. and M.O.; supervision, H.Y.; project administration, H.Y.; funding acquisition, H.Y. All authors have read and agreed to the published version of the manuscript.

Funding: This research was funded by the Bogazici University Scientific Research Fund (BAP), Istanbul, Turkey, under contract number 19061, and by the BAP Research Universities Support Program (ADP), which is supported by the Turkish Council of Higher Education (YÖK) under contract number 50005 (23AYOKADP1).

Institutional Review Board Statement: Not applicable.

Informed Consent Statement: Not applicable.

Data Availability Statement: The data are contained within the article.

Acknowledgments: The authors wish to thank in advance the anonymous reviewers for their valuable time in reviewing this paper.

Conflicts of Interest: The authors declare no conflicts of interest.

Abbreviations

AWGN: additive white Gaussian noise; BER: bit error rate; FET: field-effect transistor; FOV: field of view; ITS: intelligent transportation system; LED: light-emitting diode; NRZ: Non-Return-to-Zero; OOK: on-off keying; PHY: physical layer; PPM: Pulse Position Modulation; RF: radio

frequency; Rx: receiver; SNR: signal-to-noise ratio; Tx: transmitter; V2V: vehicle-to-vehicle; VLC: visible light communication

References

1. Căilean, A.-M.; Dimian, M. Current challenges for visible light communications usage in vehicle applications: A survey. *IEEE Commun. Surv. Tutor.* **2017**, *19*, 2681–2703. [[CrossRef](#)]
2. Bazzi, A.; Masini, B.M.; Zanella, A.; Thibault, I. Visible light communications as a complementary technology for the internet of vehicles. *Comput. Commun.* **2016**, *93*, 39–51. [[CrossRef](#)]
3. Abuella, H.; Abu-Rgheff, M.A.; Senouci, S.M. Hybrid RF/VLC systems: A comprehensive survey on network topologies, performance analyses, applications, and future directions. *IEEE Access* **2021**, *9*, 160402–160436. [[CrossRef](#)]
4. Abualhoul, M. Visible Light and Radio Communication for Cooperative Autonomous Driving: Applied to Vehicle Convoy. Ph.D. Thesis, Université Paris Sciences et Lettres, Paris, France, 2016.
5. Van Huynh, V.; Le, N.-T.; Saha, N.; Chowdhury, M.Z.; Jang, Y.M. Inter-cell interference mitigation using soft frequency reuse with two FOVs in visible light communication. In Proceedings of the 2012 International Conference on ICT Convergence (ICTC), Jeju Island, Republic of Korea, 15–17 October 2012; pp. 141–144.
6. Ghassemlooy, Z.; Arnon, S.; Uysal, M.; Xu, Z.; Cheng, J. Emerging optical wireless communications—advances and challenges. *IEEE J. Sel. Areas Commun.* **2015**, *33*, 1738–1749. [[CrossRef](#)]
7. Panta, K.; Armstrong, J. Indoor localisation using white LEDs. *Electron. Lett.* **2012**, *48*, 228–230. [[CrossRef](#)]
8. Wu, X.; Zhao, X.; Chen, M. VLC-based networking: Feasibility and challenges. *J. Netw. Comput. Appl.* **2016**, *72*, 142–153.
9. Li, X.; Wang, J. An advanced indoor optical wireless positioning system based on visible light communication using particle swarm optimization. *Optik* **2014**, *125*, 2065–2070.
10. Rahaim, M.B.; Vegni, A.M.; Little, T.D.C. A hybrid radio frequency and broadcast visible light communication system. *IEEE Globecom Work.* **2013**, 1087–1092.
11. Sharda, P.; Reddy, G.S.; Bhatnagar, M.R.; Ghassemlooy, Z. A comprehensive modeling of vehicle-to-vehicle based VLC system under practical considerations, an investigation of performance, and diversity property. *IEEE Trans. Commun.* **2022**, *70*, 3320–3332. [[CrossRef](#)]
12. Yang, Y.; Wang, J.; Shi, C. A high-efficiency LED driver with reduced flicker for visible light communication. *IEEE Photonics Technol. Lett.* **2015**, *27*, 1977–1980.
13. Pathak, P.H.; Feng, X.; Hu, P.; Mohapatra, P. Visible light communication, networking, and sensing: A survey, potential and challenges. *IEEE Commun. Surv. Tutor.* **2015**, *17*, 2047–2077. [[CrossRef](#)]
14. Ayub, S.; Kariyawasam, S.; Honary, M.; Honary, B. A practical approach of VLC architecture for smart city. In Proceedings of the 2013 Loughborough Antennas & Propagation Conference (LAPC), Loughborough, UK, 11–12 November 2013; pp. 106–111.
15. Li, D.; Xu, Z.; Zhu, H. Light positioning and indoor positioning with optical wireless communication. *J. Opt. Soc. Am. B* **2014**, *31*, 694–704.
16. Zhuang, Y.; Yang, J.; Li, Y.; Qi, L.; El-Sheimy, N. A non-line-of-sight UWB indoor positioning system using DS-TWR and IMU. *J. Navig.* **2018**, *71*, 435–452.
17. Rahman, M.T.; Bakibillah, A.S.M.; Parthiban, R.; Bakaul, M. Review of advanced techniques for multi-gigabit visible light communication. *IET Optoelectron.* **2020**, *14*, 359–373. [[CrossRef](#)]
18. Wang, X.; Huang, Z.; Huang, Y.; Chen, W. Energy-efficient adaptive modulation scheme for visible light communication. *IEEE Photonics J.* **2018**, *10*, 1–11.
19. Tanaka, Y.; Haruyama, S.; Nakagawa, M. Wireless optical transmissions with white colored LED for wireless home links. *IEEE Int. Symp. Pers. Indoor Mob. Radio Commun.* **2003**, *2*, 1325–1329.
20. Cheng, N.; Lu, N.; Zhang, N.; Shen, X.; Mark, J.W. Vehicular WiFi offloading: Challenges and solutions. *Veh. Commun.* **2014**, *1*, 13–21. [[CrossRef](#)]
21. Burchardt, H.; Serafimovski, N.; Tsonev, D.; Videv, S.; Haas, H. VLC: Beyond point-to-point communication. *IEEE Commun. Mag.* **2014**, *52*, 98–105. [[CrossRef](#)]
22. Su, Y.; Bai, H.; Zhang, R.; Wang, H. A novel dimmable visible light communication system for automotive applications. *Opt. Express* **2015**, *23*, 13607–13618.
23. Ding, J.; Guo, Z.; Lin, Y. Design and implementation of a visible light communication system for indoor positioning. *Sensors* **2018**, *18*, 2674.
24. Darak, S.J.; Jagannatham, A.K. Resource allocation in delay constrained OFDMA systems with statistical delay guarantees. *IEEE Trans. Signal Process.* **2013**, *61*, 4070–4084.
25. Căilean, A.-M.; Dimian, M. Impact of IEEE 802.15.7 Standard on Visible Light Communications Usage in Automotive Applications. *IEEE Commun. Mag.* **2017**, *55*, 169–175. [[CrossRef](#)]
26. Yamazato, T.; Takai, I.; Yendo, T.; Fujii, T.; Okada, H.; Arai, S.; Andoh, M.; Harada, T.; Yamada, K. Image-sensor-based visible light communication for automotive applications. *IEEE Commun. Mag.* **2014**, *52*, 88–97. [[CrossRef](#)]
27. Takai, I.; Inoue, K.; Kamada, S.; Fujii, T.; Igarashi, K.; Matsubara, H.; Andoh, M.; Yendo, T.; Okada, H.; Yamazato, T. LED and CMOS image sensor based optical wireless communication system for automotive applications. *IEEE Photonics J.* **2013**, *5*, 6801418. [[CrossRef](#)]

28. Căilean, A.-M.; Dimian, M. Toward environmental-adaptive visible light communications receivers for automotive applications: A review. *IEEE Sens. J.* **2016**, *16*, 2803–2811. [[CrossRef](#)]
29. Yoo, J.-H.; Kwon, D.-Y.; Won, J.-H.; Park, M.-H. Demonstration of vehicular visible light communication based on LED headlamp. *Int. J. Automot. Technol.* **2016**, *17*, 347–352. [[CrossRef](#)]
30. Avătămăniței, S.-A.; Beguni, C.; Căilean, A.-M.; Dimian, M.; Popa, V. Evaluation of misalignment effect in vehicle-to-vehicle visible light communications: Experimental demonstration of a 75 m link. *Sensors* **2021**, *21*, 3577. [[CrossRef](#)]
31. Beguni, C.; Căilean, A.-M.; Avătămăniței, S.-A.; Potorac, A.-D.; Zadobrischi, E.; Dimian, M. Increasing Vehicular Visible Light Communications Range Based on LED Current Overdriving and Variable Pulse Position Modulation: Concept and Experimental Validation. *Sensors* **2023**, *23*, 3656. [[CrossRef](#)]
32. Gurbilek, G.; Koca, M.; Uyrus, A.; Soner, B.; Basar, E.; Coleri, S. Location-aware adaptive physical layer design for vehicular visible light communication. In Proceedings of the 2019 IEEE Vehicular Networking Conference (VNC), Los Angeles, CA, USA, 4–6 December 2019; pp. 1–4.
33. Eldeeb, H.B.; Miramirkhani, F.; Uysal, M. A path loss model for vehicle-to-vehicle visible light communications. In Proceedings of the 2019 15th International Conference on Telecommunications (ConTEL), Graz, Austria, 3–5 July 2019; pp. 1–5.
34. Lee, I.E.; Sim, M.L.; Kung, F.W. Performance enhancement of outdoor visible-light communication system using selective combining receiver. *IET Optoelectron.* **2009**, *3*, 30–39. [[CrossRef](#)]
35. Momen, M.M.A.; Garg, A.K.; Fayed, H.A.; Ismail, N.E.; Mokhtar, A.; Aly, M.H. Enhanced three-lane vehicle visible light communication system. *Opt. Quantum Electron.* **2021**, *53*, 581. [[CrossRef](#)]
36. Matter, K.M.; Fayed, H.A.; El-Aziz, A.A.; Aly, M.H. Enhanced bit error rate in visible light communication: A new LED hexagonal array distribution. *Opt. Quantum Electron.* **2022**, *54*, 506. [[CrossRef](#)]
37. Mahfouz, N.E.; Fayed, H.A.; Abd El Aziz, A.; Aly, M.H. Improved light uniformity and SNR employing new LED distribution pattern for indoor applications in VLC system. *Opt. Quantum Electron.* **2018**, *50*, 350. [[CrossRef](#)]
38. Ebrahimi, F.; Ghassemlooy, Z.; Olyaei, S. Investigation of a hybrid OFDM-PWM/PPM visible light communications system. *Opt. Commun.* **2018**, *429*, 65–71. [[CrossRef](#)]
39. Loureiro, P.A.; Guiomar, F.P.; Monteiro, P.P. Visible light communications: A survey on recent high-capacity demonstrations and digital modulation techniques. *Photonics* **2023**, *10*, 993. [[CrossRef](#)]
40. MathWorks. *MATLAB. R2023b*; MathWorks: Natick, MA, USA, 2023.
41. Komine, T.; Nakagawa, M. Fundamental analysis for visible-light communication system using LED lights. *IEEE Trans. Consum. Electron.* **2004**, *50*, 100–107. [[CrossRef](#)]
42. Samsung. PixCell LED for Automotive. Available online: <https://led.samsung.com/automotive/automotive-modules/pixcell-led/> (accessed on 14 September 2024).
43. *IEEE Std 802.15.7-2011*; IEEE Standard for Local and Metropolitan Area Networks—Part 15.7: Short-Range Wireless Optical Communication Using Visible Light. IEEE: New York, NY, USA, 2011.
44. Graham, M.E. *US Department of Transportation's Vehicle-to-Everything (V2X) Communications Summit: Preparing for V2X Deployment*; US Department of Transportation: Washington, DC, USA, 2022. Available online: <https://www.nts.gov/Advocacy/Activities/Pages/Graham20220825.aspx> (accessed on 3 October 2024).
45. Toshiba Semiconductor. Reference Design: Detail RD209. *Toshiba Semiconductor and Storage*, 2022. Available online: <https://toshiba.semicon-storage.com/ap-en/semiconductor/design-development/referencedesign/detail.RD209.html> (accessed on 3 October 2024).

Disclaimer/Publisher's Note: The statements, opinions and data contained in all publications are solely those of the individual author(s) and contributor(s) and not of MDPI and/or the editor(s). MDPI and/or the editor(s) disclaim responsibility for any injury to people or property resulting from any ideas, methods, instructions or products referred to in the content.